

Volcanoes and Climate Effects of Aerosols

LEAD AUTHORS D. L. Hartmann and P. Mouginiis-Mark

CONTRIBUTING AUTHORS G. J. Bluth
 J. A. Coakley, Jr.
 J. Crisp
 R. E. Dickinson
 P. W. Francis
 J. E. Hansen
 P. V. Hobbs
 B. L. Isacks
 Y. J. Kaufman
 M. D. King
 W. I. Rose
 S. Self
 L. D. Travis

CHAPTER 8 CONTENTS

8.1	Importance of volcanoes, natural aerosols, and anthropogenic aerosols	341
8.2	Major scientific questions and hypotheses	342
8.2.1	Stratospheric volcanic aerosols and climate	342
8.2.1.1	Source gases for stratospheric aerosols	342
8.2.1.2	Explosiveness and plume history during individual eruptions	343
8.2.1.3	Frequency of eruptions, tectonic setting, rock/ash vs. SO ₂	343
8.2.1.4	Gas-to-particle conversion and removal mechanisms	343
8.2.1.5	Radiative properties and climatic effects of stratospheric aerosols	345
8.2.1.6	Needed satellite and in situ measurements	347
8.2.1.6.1	Global observations of stratospheric aerosol optical properties	347
8.2.1.6.2	Lidar measurements of aerosols	347
8.2.2	Volcanic aerosols and stratospheric ozone depletion	349
8.2.3	Climatic effects of tropospheric aerosols	349
8.2.3.1	Natural emission of tropospheric aerosols	349
8.2.3.2	Anthropogenic sources of aerosols	350
8.2.3.2.1	Sulfur emission and oxidation to sulfate particles	351
8.2.3.2.2	Biomass burning	351
8.2.3.3	Direct radiative effects of tropospheric aerosols	352
8.2.3.4	Indirect effects of aerosols on cloud abundance, lifetime, and optical properties	354
8.2.3.5	Science investigations using EOS data	355
8.2.3.6	Needed satellite and in situ measurements	355
8.2.3.6.1	Global observations of tropospheric aerosol optical properties	355
8.2.3.6.2	Surface monitoring of tropospheric aerosols	357
8.2.3.6.3	Intensive field campaigns	358
8.2.4	Volcanic hazards	358
8.2.4.1	Health hazards of tropospheric volcanic gases and aerosols	359
8.2.4.2	Lava flows and volcanic mud flows	361
8.2.4.3	Hazards to aircraft from eruption plumes	361
8.2.4.4	Needed satellite and in situ measurements	361
8.3	Required measurements and data sets	362
8.3.1	Stratospheric aerosols	362
8.3.2	Tropospheric aerosols	364
8.3.3	Volcanic aerosol precursor gases	364
8.3.4	Volcanic hazards	364
8.3.5	Importance of measurements collected by the missions of foreign partners	366
8.4	EOS contributions: Expected improvement in knowledge and national benefit	367
8.4.1	Monitoring of volcanic eruptions and aerosols and their effects on climate	367
8.4.2	Improved assessment of volcanic hazards on the ground and in the air	367
8.4.3	Improved knowledge of the global frequency and magnitude of volcanic eruptions	368
8.4.4	Global measurements of tropospheric aerosols	368
8.4.5	Assessment of the role of tropospheric aerosols in climate change	370
8.4.6	Inclusion of aerosol effects in model predictions of global climate change	371
8.4.7	Advertent climate modification by aerosols	372
	References	373
	Chapter 8 Index	378

8.1 Importance of volcanoes, natural aerosols, and anthropogenic aerosols

Volcanoes have a significant effect on the global environment. In the long term, they affect the gaseous composition of the atmosphere by emitting gases from the interior of the Earth and play a key role in the evolution of the Earth's atmosphere and climate. Variations in the output of volcanoes can cause variations of climate on a variety of time scales. It has been demonstrated that a sufficiently violent eruption can cause a measurable change in the Earth's climate with a time scale of a few years. The magnitude of the temperature change depends on the amount of sulfur that is injected into the stratosphere, among other factors. The sulfur gases are oxidized to sulfuric acid aerosols in the stratosphere, where they may reside for a year or more before being flushed out by sedimentation and the fluid motions of the stratosphere. Generally, a surface cooling is produced by these aerosols, because they reduce the amount of solar radiation reaching the surface more than they reduce the amount of escaping longwave emissions. It is conceivable that a modulation in the frequency of this type of eruption on time scales of decades or longer could cause a variation of the Earth's climate on the same time scale.

The periods of cooling associated with major eruptions must be accounted for in efforts to detect trends that might be associated with increasing greenhouse gases or other anthropogenic climate forcings. An important challenge to the research effort on global change, for the purpose of making policy decisions, will be the early detection and quantification of climate changes caused by human activities. It is essential to recognize and remove effects resulting from natural phenomena, of which volcanic aerosols are a significant example. We are still a long way from understanding fully the effects of volcanic eruptions on atmospheric composition, climate, and weather.

In addition to their effects on atmospheric composition and global climate, volcanic eruptions have effects in shaping the local landscape and can pose a serious hazard to life and property in their vicinity.

Volcanic emissions and resulting stratospheric aerosols can also have an important influence on stratospheric chemistry, both through chemical reactions that

take place on the surfaces of aerosols and through the temperature changes that aerosols can induce in the stratosphere. Stratospheric aerosols can result in heating of the stratosphere, which can have significant effects on stratospheric dynamics and transport.

Aerosols in the troposphere are also important for global climate. A wide variety of aerosol types exists, including sea salt and dust carried from the surface into the atmosphere by wind, and aerosols formed by chemical transformation from gaseous compounds to molecules that exist in solid or liquid form. In the upper troposphere, a significant fraction of the aerosol burden can come from advection or sedimentation from the stratosphere. The sources of aerosols are both natural and anthropogenic. Although the lifetime of aerosols in the troposphere is only a few weeks, the sources are strong enough to maintain a significant aerosol burden. The aerosols contributed by humans have been increasing, particularly those associated with sulfur dioxide (SO_2) released during the combustion of coal, petroleum, and biomass. It is currently estimated that the anthropogenic source of sulfuric acid aerosols in the troposphere is greater than the natural source. The primary effect of these aerosols is to cool the Earth by reflecting solar radiation, either directly, or by becoming incorporated into small cloud droplets or ice crystals. It is estimated that the direct effect of sulfate aerosols produced by humans on the Earth's energy balance is currently about -0.5 Wm^{-2} , compared to the forcing associated with the change in greenhouse gases during the industrial age of about $+2 \text{ Wm}^{-2}$. The indirect effect of human-produced aerosols on the properties of clouds may be of the same order, making tropospheric aerosols one of the major uncertainties in understanding climate change.

It is important to obtain accurate measurements of aerosols not only because of their importance for climate, but also to allow a higher degree of accuracy in remote sensing of surface properties such as sea surface temperature (SST), ocean color, and land surface properties. During major volcanic eruptions, satellite monitoring of stratospheric chemical and physical properties is also significantly affected by aerosols.

8.2 Major scientific questions and hypotheses

8.2.1 Stratospheric volcanic aerosols and climate

The year 1816, “the year without a summer,” is probably the best known putative example of a volcanically-induced climate cooling event. It was largely caused by the eruption of Tambora, Indonesia, in April 1815. Tambora erupted an estimated 50 cubic kilometers of magma and produced 100 megatons of sulfuric acid aerosols, in one of the largest known volcanic eruptions of the past few millennia. The aerosol veil caused cooling of up to 1°C regionally and probably more locally, with effects lasting until the end of 1816 and extending to both hemispheres. It snowed in New England in June, and abnormally low temperatures in Europe led to widespread famine and misery, although the possible connection to volcanic aerosols was not realized at the time.

Scientists first recognized and observed volcanic atmospheric dust veils after the eruption of Krakatau, Indonesia, in 1883, and it was then thought that fine-grained silicate dust was the cause of the atmospheric perturbations. However, since the discovery of the stratospheric sulfate aerosol layer in the 1960s, it has become evident that this layer in the atmosphere, which plays a large role in modulating the net incoming radiation, is strongly influenced by volcanogenic sulfide released from the magma.

Several recent eruptions have proven invaluable in improving our understanding of the connections among volcanism, aerosols, and climate change. Two eruptions of very sulfur-rich magma at El Chichón, Mexico, in 1982 and Mount Pinatubo, in Luzon, Philippines, in 1991 have been well documented in terms of the stratospheric aerosols produced, their spread and atmospheric residence time, and their climatic effects. El Chichón was a small-volume eruption of unusually sulfur-enriched magma that produced the first large aerosol veil to be tracked by instruments on satellites. Its impact on surface temperatures has, however, been difficult to assess. Pinatubo was the second-largest eruption in the twentieth century (the largest was Mt. Katmai in Alaska in 1912), and its aerosol veil enveloped the Earth for more than 18 months, causing spectacular sunrises and sunsets worldwide. There was more material in the aerosol layer than at any time since Krakatau erupted. General circulation models (GCMs) of temperature changes expected under this aerosol cloud predicted Northern Hemisphere surface cooling of as much as 0.5°C, and changes of this order are consistent with the meteorological data.

Recent studies have established a strong correlation between certain types of eruptions and climate change,

and it has been suggested that there may be a simple relationship between the sulfur yield of a volcanic eruption and decreases in surface temperature. It is known that enhanced levels of aerosols after volcanic eruptions coincide with periods of lowered incident solar radiation, lower surface and tropospheric temperatures, and stratospheric warming. The magnitude of the signal in the surface temperature record is difficult to detect against background variation, however, even for the largest historic eruptions. Recently, it has been suggested that for the Agung (1964) and El Chichón (1982) cases, subtracting the warming effects of El Niño from the temperature record makes the volcanic signal clearer. Simple models suggest that eruptions on the scale of large prehistoric events have the potential to alter climate to a much greater degree than has been observed following volcanic events in the historical record.

8.2.1.1 Source gases for stratospheric aerosols

Sulfur is released into the atmosphere during eruptions mainly as SO₂ gas, which is converted by photochemical oxidation to sulfuric acid (H₂SO₄) via OH. Sometimes H₂S can be the dominant sulfur-bearing gas species in an eruption cloud (Hobbs et al. 1981; Kotra et al. 1983). Sulfuric acid (70%) and water (30%) are the dominant components of the resulting aerosols. Aerosols form liquid spheres (~0.3 μm modal radius), with solid silicate (ash) cores dominant in the first month. Atmospheric residence time ranges from days to years, depending on particle size, injection history, and location of the aerosol in question.

Injection of other volatiles such as HCl and H₂O may alter atmospheric composition as well, but evidence for long-term residence of Cl compounds from volcanic HCl emission is lacking. Aerosol composition is further altered by heterogeneous reactions on sulfate aerosol surfaces.

SO₂ has been recognized as the major contributor to stratospheric aerosols. Based on magma chemistry, it is poorly known why other gases, and HCl in particular, are not injected into the stratosphere during violent volcanic eruptions. Some form of “scavenging mechanism” seems to exist wherein, perhaps, water vapor leaches out these other gases during plume ascent rather than allowing the gases to be injected into the stratosphere. The mechanism wherein separation of the ash from the gases within the plume takes place also needs to be understood. Detailed satellite observations of the plume are needed to help resolve this issue, as well as understand the dissipation of energy from the plume into the atmosphere.

8.2.1.2 *Explosiveness and plume history during individual eruptions*

Through study of historic eruptions and their atmospheric impacts, we have learned what types of eruptions can influence the Earth's climate. Climatic effects appear to ensue if the eruption cloud is powerful enough to inject material into the stratosphere, or if the eruption is of sufficient duration that a higher-than-normal level of tropospheric aerosols is maintained. The impact on climate also depends on the sulfur content of the magma: some volcanoes erupt sulfur-rich magmas, some magma with average amounts, and some magma with low sulfur content. The ultimate source of volcanic sulfur is yet to be determined: some may be primordial and some may be recycled in the Earth's lithosphere. If an eruption is large enough, even with a low magmatic sulfur content, sufficient magma is erupted to cause a significant release of sulfur gas, leading to the generation of aerosol particles.

8.2.1.3 *Frequency of eruptions, tectonic setting, rock/ash vs. SO₂*

Determining how large an impact an eruption can have on climate is a major issue. Volcanic eruptions are known to affect surface temperature, precipitation, and weather patterns, but what has not been studied in detail are either the short-term (1-3 years) effects of individual events, or the longer-term (10-50 years) changes that might be controlled by periods of enhanced volcanism. Although the greater the eruption, the lower the frequency of occurrence, eruptions have a frequency that varies according to type and magnitude of the event. We have an imperfect record of past eruptions and changes in temperature and weather. Future events will provide natural experiments in which we can study the impact of volcanic aerosols, an effort already begun.

Significant eruptions, and therefore aerosol clouds, occur every 10-20 years on average, with a major eruption perhaps every 100 years. Latitude and time of year of eruptions influence dispersal of volcanic aerosol clouds. Some magmas are richer in sulfate than others (e.g., El Chichón), but the duration of the eruption is also important for climate modification (e.g., 1783 Laki fissure eruption in Iceland).

8.2.1.4 *Gas-to-particle conversion and removal mechanisms*

The aerosol loading of the stratosphere is strongly driven by periodic volcanic eruptions that can produce a significant perturbation to the Earth-atmosphere system by injecting material into the stratosphere where, depending on the magnitude and altitude of the injection, it may per-

sist for several years. The material injected into the stratosphere may include ash, which typically does not remain for more than a few months, and gaseous components including water vapor and SO₂. Aerosols are produced when the SO₂ is chemically transformed into sulfuric acid (H₂SO₄), which rapidly condenses into aerosols since it has a very low saturation vapor pressure (McCormick et al. 1995). Additional sources of stratospheric aerosols include natural (e.g., biogenic Carbonyl Sulfide [COS]) and anthropogenic sources (e.g., SO₂ from industry and aviation).

The introduction of large amounts of sulfuric acid aerosol by a volcano into the stratosphere increases the planetary albedo, since these aerosol particles are efficient scatterers, but only weak absorbers, at solar wavelengths. For instance, following the eruption of Mt. Pinatubo, an analysis of data from the Earth Radiation Budget Experiment (ERBE) found that the albedo in July, August, and September 1991 increased to 0.250 from a 5-year mean of 0.236 (Minnis et al. 1993). To a first approximation, an increase in stratospheric opacity, such as that following the eruption of Mt. Pinatubo, should cool the Earth as the aerosol increases the albedo of the Earth-atmosphere system and therefore increases the amount of solar radiation scattered back into space. However, microphysical properties of the aerosol (in particular, aerosol size) determine whether the infrared absorptivity of stratospheric aerosols, which acts to warm the Earth, dominates the scattering of incoming solar radiation back into space (i.e., the albedo effect), which acts to cool the Earth (e.g., King et al. 1984). It has been shown (Lacis et al. 1992) that if the aerosol effective radius (i.e., the area-weighted mean radius of the aerosol size distribution) exceeds ~2 μm, the warming effect overrides the cooling effect. Following the Pinatubo eruption, measurements indicated an increase in the average particle radius from 0.3 μm prior to the eruption to about 1 μm after the eruption; thus cooling would be expected (Russell et al. 1993a, b; Thomason 1992; Grainger et al. 1995). The average size of volcanic aerosols varies with position and time after the eruption, but the dominant effect at the surface appears to be cooling.

Substantial heating in the stratosphere was observed immediately after the eruptions of El Chichón and Mt. Pinatubo (Labitzke et al. 1983; Labitzke and McCormick 1992). In the case of Mt. Pinatubo, this heating was sufficient to cause tropical stratospheric temperatures to increase by as much as three standard deviations above the 26-year mean at 30 hPa (~24 km). Analyses using the satellite-borne Microwave Sounding Unit (MSU) also indicate higher-than-average stratospheric temperatures in 1991 and 1992. By the end of

1993, however, stratospheric temperatures had decreased to the lowest values ever observed by MSU. This cooling may be related to the ozone loss observed in the stratosphere, since ozone is an effective absorber of solar radiation and is responsible for substantial heating in the stratosphere. The observed ozone loss was probably due in large part to heterogeneous chemical reactions on Pinatubo aerosols.

The negative radiative forcing associated with the eruption of Mt. Pinatubo exceeded the magnitude of the positive forcing associated with greenhouse gases during the second half of 1991 and much of 1992, and remained significant through 1993. In response to this forcing, the 1992 tropospheric temperature anomaly, adjusted for the effects of El Niño-Southern Oscillation (ENSO) variations, was -0.4°C , a decrease of more than 0.7°C from 1991 (Halpert et al. 1993). Data from MSU (Dutton and Christy 1992) yield a similar global decline in lower tropospheric temperatures of 0.5°C in mid-1992 with much of the decrease occurring in the Northern Hemisphere (0.7°C). In a globally averaged sense, the measured temperature anomaly is consistent with the value of -0.5°C estimated from a global climate model (Hansen et al. 1992). The departure is also comparable to the estimated impact of Tambora in 1815 (-0.4 to -0.7°C) and greater than that estimated for El Chichón in 1982 (-0.2°C) and Krakatau in 1883 (-0.3°C). It is surprising that the Pinatubo cooling exceeded that of Krakatau, since the latter is believed to have injected more SO_2 into the stratosphere. However, this anomaly may simply reflect uncertainties in the estimates of both stratospheric aerosol loading and global surface temperature, particularly for the earlier eruption. It should be noted that the small mean changes in global temperature are not evenly distributed, but consist of regions of both relative cooling and warming, the locations and magnitudes of which are dependent on season.

Injection of volcanic aerosol at high latitudes appears to be fairly well confined to the hemisphere of the injection, such as was observed following the eruption of Mt. St. Helens in May 1980. Volcanic injections at low latitudes and high altitudes exhibit relatively slow transport time scales of volcanic material out of the tropics to both hemispheres. Observations following the eruptions of El Chichón in 1982 and Nevada del Ruiz in 1985 revealed the presence of enhanced reservoirs of volcanic aerosol at low latitudes that persisted for several years (Yue et al. 1991). Poleward transport of aerosol into the winter hemisphere tends to be suppressed when easterly winds lie over the equator. During these conditions, strong horizontal wind shear lies in the subtropics, separating

the tropical easterlies and extratropical westerlies in the winter hemisphere. Large-scale potential vorticity gradients associated with these shears inhibit the horizontal mixing of air. When westerly winds lie over the equator, however, horizontal wind shear is weaker in the subtropics and meridional mixing occurs more readily. The reversal between easterly and westerly winds in the lower tropical stratosphere (the Quasi-Biennial Oscillation or QBO) dominates the circulation in the tropical stratosphere and has a period of approximately 28 months.

A similar signature of relatively slow tropical aerosol transport to high latitudes was evident after the eruption of Mt. Pinatubo. Easterly winds prevailed above 23 km in the lower tropical stratosphere for the first six months after the eruption. Above this height, airborne lidar (Winker and Osborn 1992) and satellite (Trepte and Hitchman 1992) observations of the volcanic plume found steep meridional gradients of aerosol near 20°N and 20°S . The tropical confinement of aerosol gives rise to a long-lived, zonal-banded pattern in stratospheric optical thickness following low-latitude eruptions (Trepte et al. 1994; Long and Stowe 1994; Grant et al. 1996). At lower altitudes, however, volcanic aerosol disperses more quickly poleward, and it was primarily this low-altitude transport that was responsible for the initial lidar observations of the Pinatubo aerosol in northern midlatitudes shortly after the eruption (e.g., Post et al. 1992).

Over the course of time, volcanic aerosol is transported from the stratosphere into the troposphere where a variety of mechanisms (mostly associated with clouds and precipitation) are effective in the deposition of the aerosol to the Earth's surface. Increasing the number of aerosol particles available to act as cloud condensation and ice nuclei tends to reduce the mean size of the resulting cloud particles. Since smaller particles are more efficient scatterers of visible radiation, this process increases the albedo of the cloud. It has been suggested that optically-thin (but radiatively important) cirrus (Sassen et al. 1995) and deep convection clouds may be subject to similar microphysical changes. Although it is not clear if any changes in the optical properties of cirrus following a volcanic eruption have been observed, Song et al. (1996) show an apparent effect of Pinatubo aerosols on high cloudiness of moderate or greater optical depths, as measured by the pattern of the outgoing longwave radiation (OLR) anomaly, that lasted for several years after the eruption. Gravitational sedimentation of the aerosol, subsidence in the winter hemisphere (particularly within the polar vortices), and episodic transport of stratospheric air into the troposphere through tropopause folds are responsible for the removal of aerosol from the stratosphere. Following the June 1991

eruption of Mt. Pinatubo, the total stratospheric aerosol mass decreased with an e-folding time of approximately one year.

The Mt. Pinatubo eruption is the best observed example of an explosive eruption with global effects. The large Pinatubo stratospheric SO₂ cloud began to spread rapidly and oxidize to form stratospheric sulfuric acid aerosols (Figure 8.1). About half of the SO₂ had been converted to sulfuric acid aerosols by four weeks after the eruption (Winker and Osborn 1992). The Microwave Limb Sounder (MLS) on the Upper Atmosphere Research Satellite (UARS) satellite detected minor amounts of unoxidized SO₂ for up to 170 days after the eruption. Accordingly, the average conversion time of SO₂ is about 33 days (Read et al. 1993). Multiwavelength stratospheric aerosol extinction measurements from the SAGE II and airborne and ground-based photometers revealed greatly

mained near the equator 4-5 months after the eruption (Figure 8.2, pg. 346). The typical size of volcanic aerosols observed several months following the eruption was in the range of 0.3 to 0.5 μm (Deshler et al. 1992a, 1993; Pueschel et al. 1992; Asano 1993; Asano et al. 1993), and aerosol size appeared to be a strong function of latitude and altitude (Grainger et al. 1995; Lambert et al. 1993). Numerical modeling has reproduced the observed microstructure and optical properties of the Pinatubo aerosols during the period of their formation and growth in the stratosphere (Zhao et al. 1995).

8.2.1.5 Radiative properties and climatic effects of stratospheric aerosols

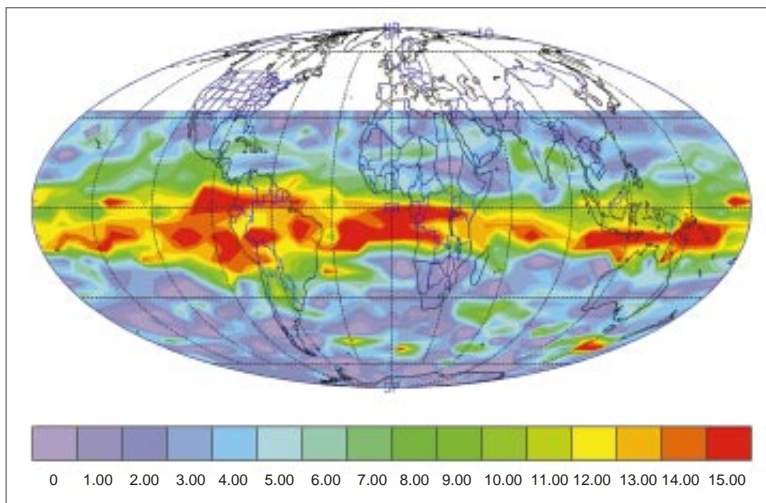
Temporal variations of stratospheric aerosols alter both the solar radiative cooling of the Earth-atmosphere system and the thermal emission from the Earth to space.

Thus, determination of the climate forcing caused by stratospheric aerosols requires a knowledge of aerosol properties sufficient to define their influence on both solar and terrestrial spectra. Radiative transfer tools are available for accurately simulating the climate forcing by aerosols of known size and composition. Coakley and Grams (1976), Harshvardhan and Cess (1976), and Pollack et al. (1976) were among the first to realistically portray the effect of stratospheric aerosols on both solar and terrestrial radiation.

A comprehensive illustration of how radiative forcing by stratospheric aerosols depends upon aerosol properties was provided by Lacis et al. (1992). The principal parameter is the aerosol optical

thickness, including its geographical distribution. The climate forcing also depends substantially on the effective radius of the particle size distribution. The radiative forcing is less sensitive to other characteristics of the size distribution, the aerosol composition, and the altitude of the aerosols. However, the radiative forcing, specifically the radiative flux change at the tropopause caused by the aerosols, does not completely define possible climate influence. Empirical studies (Kodera and Yamazaki 1994) and model analyses (Graf et al. 1993) suggest that changes in stratospheric temperature gradients can alter surface climate; thus, factors that influence stratospheric heating, such as aerosol composition, may also be important.

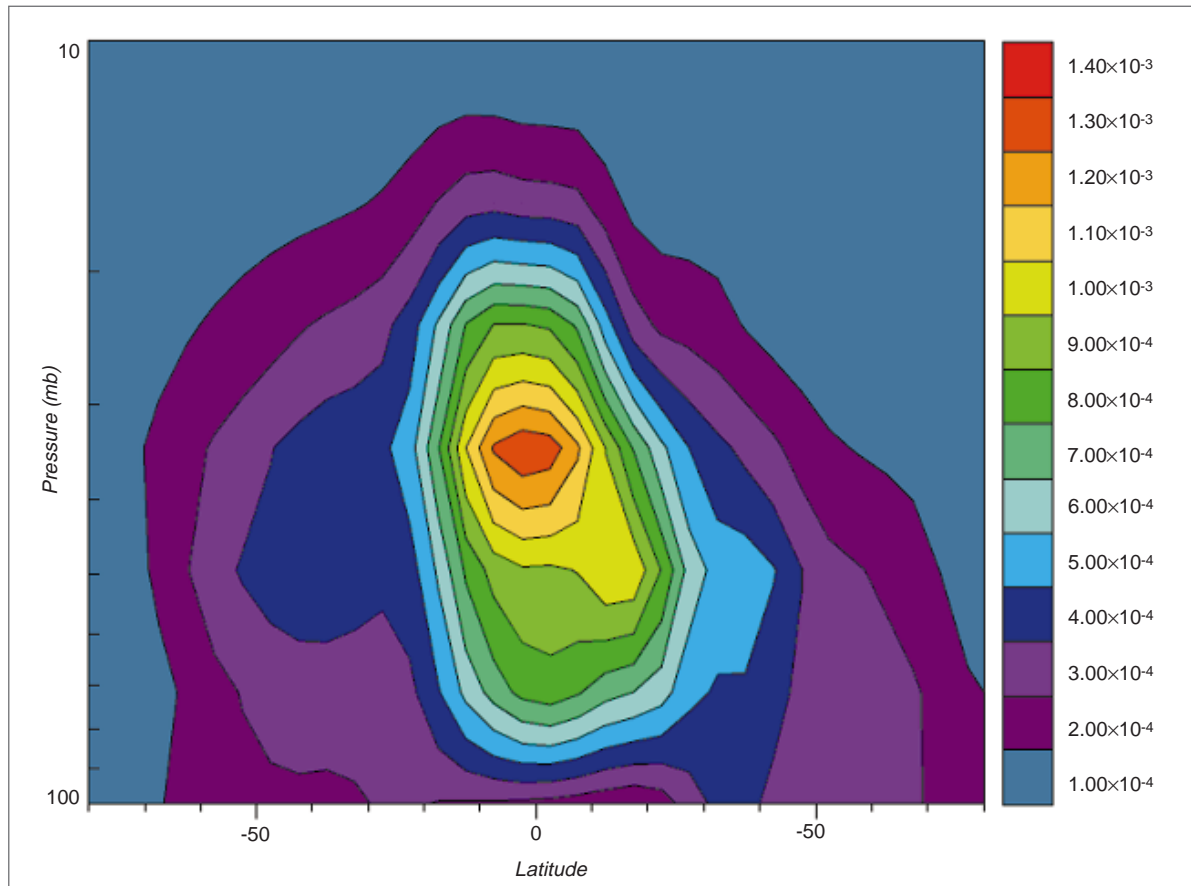
FIGURE 8.1



Map of the Mt. Pinatubo SO₂ cloud from MLS (Read et al. 1993).

increased extinction with an initial wavelength dependence indicating the presence of very small aerosols created by gas-to-particle conversion (Thomason 1992; Valero and Pilewskie 1992; Russell et al. 1993b; Dutton et al. 1994). These newly formed aerosols grew to larger sizes by condensation of sulfuric acid and water vapor and by the coagulation process (Russell et al. 1993a, b; Dutton et al. 1994), leading to optical-thickness spectra that peaked at midvisible (~0.5 μm) or longer wavelengths, starting about two months after the eruption. Over 90% of the particles collected from the volcanic clouds were composed of an H₂SO₄/H₂O solution (Deshler et al. 1992b). The highest concentration of aerosols re-

FIGURE 8.2



Zonal cross section of stratospheric zonal mean aerosol extinction for 8-11 November 1991 retrieved from atmospheric limb observations of the 12.1- μm aerosol emission of the Improved Stratospheric and Mesospheric Sounder on the Upper Atmosphere Research Satellite (Grainger et al. 1993).

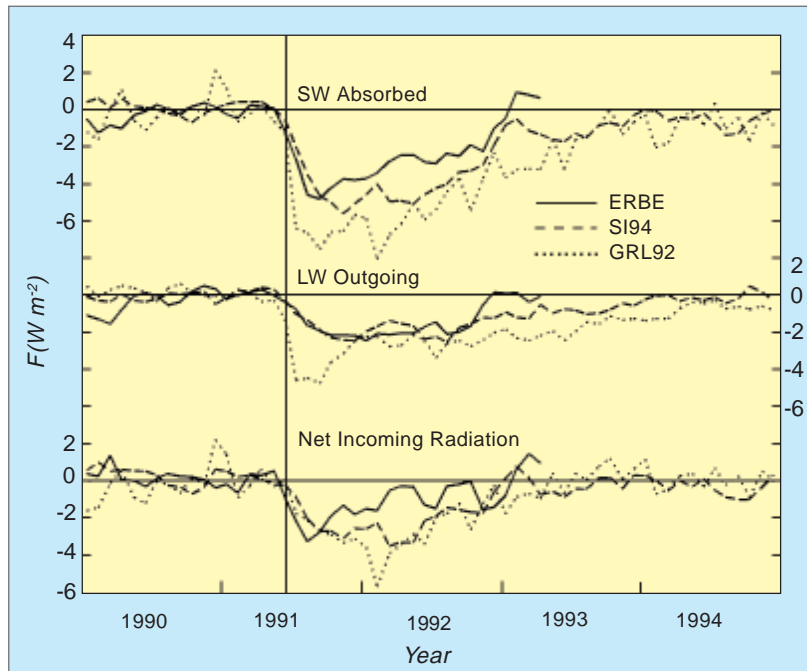
Aerosol heating can also affect the circulation of the stratosphere (Eluszkiewicz et al. 1996).

The aerosol radiative forcing resulting from the Mt. Pinatubo eruption is known much better as compared to previous large volcanic eruptions, principally because global satellite data were available for both solar spectra (especially the Stratospheric Aerosol and Gas Experiment [SAGE] II data; McCormick et al. 1995) and terrestrial spectra (especially Improved Stratospheric and Mesospheric Sounder [ISAMS] data; Grainger et al. 1993). About 20 to 30 Tg ($\text{Tg} = 10^{12} \text{ g}$) of new aerosol produced by the Pinatubo eruption was estimated by use of SAGE II (McCormick and Veiga 1992; McCormick et al. 1995), Cryogenic Limb Array Etalon Spectrometer (CLAES), and ISAMS data (Lambert et al. 1993). The mean mass, about 25 Tg of sulfate aerosol, requires that only 13 Tg of SO_2 are available to form it, if it is assumed that the aerosols are 75% H_2SO_4 and 25% H_2O (Hamill et al. 1977).

This estimate is somewhat smaller than those of SO_2 release. Infrared absorption by the Pinatubo aerosol also suggests that the composition is 59-to-77% H_2SO_4 , with the remainder being water (Grainger et al. 1993).

These satellite data have been used to infer aerosol optical thickness and effective radius of the Pinatubo aerosols as a function of time (Hansen et al. 1995), and in turn the aerosol properties have been used in the Goddard Institute for Space Studies (GISS) GCM to calculate the radiative flux anomalies at the top of the atmosphere for comparison with ERBE data (Figure 8.3). The observed flux anomaly is somewhat smaller than calculated in the model, but is probably consistent with measurement uncertainty. Both the observations and model imply a smaller forcing than was assumed in calculations immediately following the eruption (Hansen et al. 1992), which in large part accounts for the predicted cooling being somewhat greater than observed.

FIGURE 8.3



Radiation balance anomalies observed by ERBE for latitudes 40°S - 40°N (Minnis *et al.* 1993), with the mean for the period 1985-1989 to remove the seasonal cycle and with the zero point defined by the mean anomaly for the 12 months preceding the month of the Mt. Pinatubo eruption. Model radiation balance anomalies are from the simulations of Hansen *et al.* (1992) and from current simulations with the SI94 climate model and the SI94 aerosols. (GRL92 refers to a model in which the radiation balance anomalies observed by ERBE are compared with the same quantities calculated in the climate simulations of Hansen *et al.* 1992.) (courtesy of James Hansen [Goddard Institute of Space Studies]).

When more fully analyzed, the Pinatubo eruption may improve our understanding of the sensitivity of climate to aerosols. However, because of the difficulty of separating a forced climate response from natural variability, definitive conclusions will probably require analysis of additional future volcanic eruptions. Thus, it is important to maintain over decades the measurement capabilities for stratospheric aerosols and other climate forcings.

8.2.1.6 Needed satellite and in situ measurements

8.2.1.6.1 Global observations of stratospheric aerosol optical properties

Spaceborne solar and lunar occultation measurements will be made during the EOS era using SAGE III, flying in a polar orbit (Meteor 3M-1), a mid-inclination orbit (Flight of Opportunity), and a low-inclination precessing orbit (International Space Station). These data will be used to derive vertical profiles of aerosol extinction coefficient and effective particle size, as well as a number of gaseous species, thereby extending the valuable solar occultation

measurements begun by the Stratospheric Aerosol Measurement (SAM) II, SAGE, and SAGE II satellite missions. The addition of lunar occultation on SAGE III will permit more occultations to be obtained than are possible with solar occultation alone, thereby increasing the sampling opportunities. Previous records of the global distribution and dispersion of stratospheric aerosol, obtained from the mid-inclination SAGE II on the Earth Radiation Budget Satellite (ERBS), have demonstrated the magnitude and spatial distribution of stratospheric aerosols as they dispersed globally following major volcanic eruptions. Figure 8.4 (pg. 348) shows a time series of stratospheric aerosol optical thickness preceding, immediately following, and 18 months after the eruption of Mt. Pinatubo.

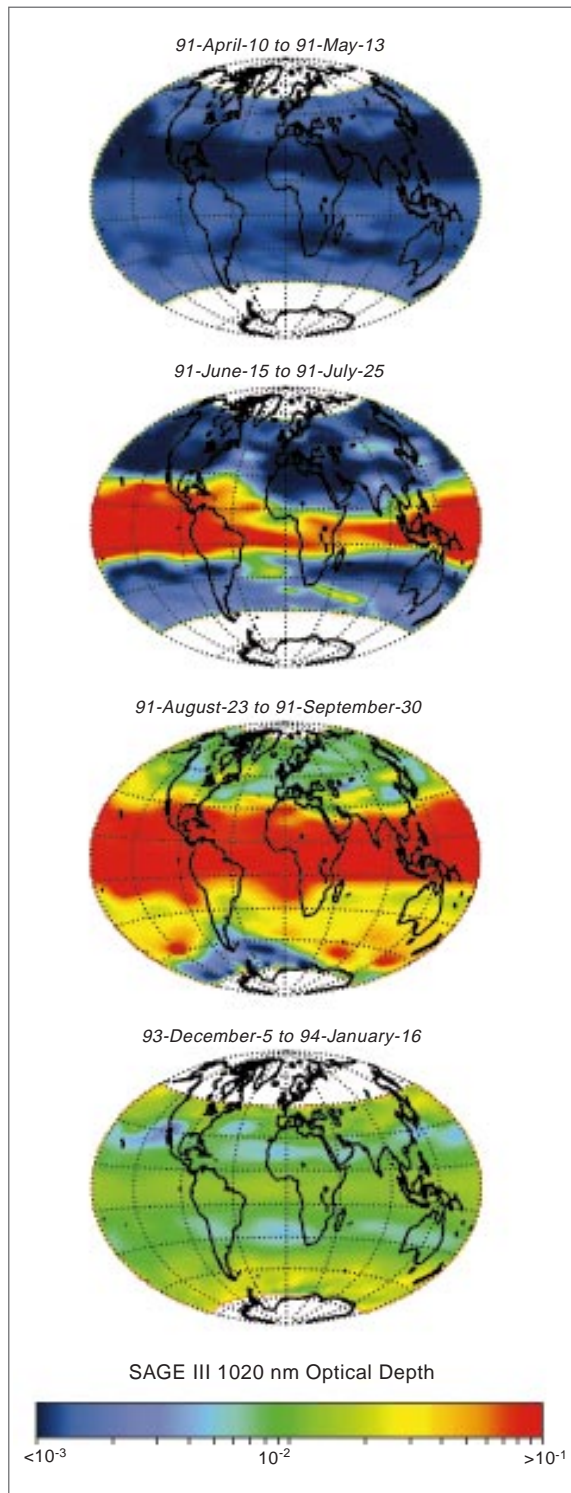
In addition to SAGE III, the High-Resolution Dynamics Limb Sounder (HIRDLS) on the Earth Observing System (EOS)

Chemistry-1 platform will be very sensitive to vertical profiles of stratospheric aerosol. HIRDLS has specifically-designed channels at 7.1, 8.3, 12.0, and 17.4 μm to sense the presence and optical properties of stratospheric aerosol through thermal emission using a limb-sounding technique. This will provide three-dimensional fields of the entire globe for altitudes above about 5-7 km under most atmospheric conditions, and the sensitivity will include particles smaller than 0.1 μm found in the midstratosphere. The vertical resolution will be 1 km, and by using an azimuth scanning capability with profiles measured every 10 seconds, a horizontal resolution of $5^{\circ} \times 5^{\circ}$ (averaging about 400 km \times 400 km) will be obtained, with a complete 3-D field twice per day. The UARS ISAMS and CLAES instruments, which both had poorer spatial resolutions, showed that the technique is highly effective for measuring the evolution of aerosol fields.

8.2.1.6.2 Lidar measurements of aerosols

Ground-based and airborne lidar measurements have made important contributions to our knowledge of stratospheric aerosol behavior in two main areas. The first of these con-

FIGURE 8.4



Aerosol optical depth measured by SAGE III before and after the eruption of Mt. Pinatubo on June 15, 1991 (P. McCormick).

cerns the long-term monitoring of the aerosol optical scattering characteristics from ground-based locations. At least two lidar stations now exist where measurements have been made continually from a single observing site for over twenty years (Osborn et al. 1995; Simonich and Clemesha 1995). These records show the injection of material by various volcanic eruptions, the earliest being that of Fuego in 1974, and the most recent and powerful being that of Pinatubo in 1991. The stratospheric effects of a number of other eruptions, many of them with much smaller impact, are clearly visible in these records. These data are the most extensive of a much larger number of data sets obtained from a global lidar network (McCormick 1993) that extends back to the mid 1960s. Taken together, these measurements form a valuable tool for examining the long-term global behavior of aerosols, particularly in terms of the magnitude and location of the volcanic sources and the dispersion and loss from the stratosphere of the injected material. Traditional wavelengths used for these systems have been in the visible or near infrared. The recent addition of CO₂ lidars operating near 10 μm has enabled the seasonal loss of stratospheric volcanic aerosols to the upper troposphere to be followed (Post 1986; Post et al. 1992), where they may be responsible for indirect radiative effects via aerosol modification of high-cloud characteristics. Lidar systems offer a high vertical resolution, allowing structures to be studied with vertical dimensions as small as a few meters. The use of multiple wavelengths provides information on particle size, allowing calculations to be made of mass loading and surface area. These quantities, or the multi-wavelength backscatter cross sections, may then be used as a basis for calculation of the radiative characteristics at other wavelengths.

The second main area in which lidars have been used to study stratospheric aerosols has been their use in airborne systems. The recent satellite-borne Lidar In-Space Technology Experiment (LITE) may be regarded as an extension of such systems. Airborne systems permit the study of the horizontal distribution of stratospheric aerosols, the extent of such studies being only limited by the cost and logistics of operating the platforms. These flight experiments have been unique in the detail they have shown of the horizontal and vertical structure of the stratospheric aerosol, providing insight into the dynamical processes responsible for producing and/or maintaining this structure. Such missions have normally been dedicated to the study of specific phenomena of interest (e.g., post-volcanic plumes [Winker and Osborn 1992] or polar stratospheric clouds [McCormick et al. 1993]). Airborne lidar measurements have also provided unique information on the transfer of material from the stratosphere to

the troposphere, showing the downward transfer of aerosol within tropopause fold structures (Browell et al. 1987). In addition to their direct application to the study of stratospheric aerosols, airborne lidars have an extensive history as validation instruments for SAM II, SAGE, and SAGE II aerosol measurements.

It is possible for an airborne lidar to map the aerosol distribution over a wide latitude range within a period of hours or days. This represents an order-of-magnitude improvement in time resolution over a satellite occultation instrument such as SAGE II or SAGE III, where the measurement location changes latitude relatively slowly with orbital drift and season, and less than 50 profiles can be obtained each day. An even more global and quasi-instantaneous picture can be obtained from a spaceborne lidar. In September 1994, LITE (McCormick 1995), operating over a 10-day period, provided a unique data set that included measurements on stratospheric aerosols, with 100° of latitude being covered in about 20 minutes.

Lidar measurements in support of EOS goals will be conducted with the Geoscience Laser Altimeter System (GLAS). The existing global ground-based network is strongly biased towards the Northern Hemisphere. More observing sites are required in both the tropics and the Southern Hemisphere. The lack of data within the equatorial reservoir zone is particularly noteworthy: no systematic stratospheric measurements have been made closer to the equator than 18° latitude. Improvements are also desirable in measurement techniques and data handling for low aerosol loadings. Lidar provides good and often unique data at times of strong volcanic activity. Technical improvements would allow lidar to contribute more readily to the important question of whether there is a long-term trend in this background concentration of stratospheric aerosol.

8.2.2 *Volcanic aerosols and stratospheric ozone depletion*

It has been realized recently that depletion of stratospheric ozone in temperate latitudes occurs after volcanic aerosol injections. Processes involving sulfate aerosols as sites for heterogeneous chemical reactions similar to those involving chlorine, which are thought to cause the ozone hole, are implicated. The role of stratospheric aerosols in ozone photochemistry is discussed in more detail in Chapter 8.

8.2.3 *Climatic effects of tropospheric aerosols*

Tropospheric aerosols affect the radiative forcing of climate through three primary mechanisms:

- 1) Direct forcing, in which radiation is scattered or absorbed by the aerosol itself. Scattering of shortwave radiation produces enhanced reflection of the Earth-atmosphere-ocean system (thereby increasing the planetary albedo), while longwave absorption enhances the atmospheric greenhouse effect. Absorption of solar and longwave radiation alters the atmospheric heating rate and may result in circulation changes;
- 2) indirect forcing, in which enhanced concentrations of aerosol particles result in enhanced concentration of cloud drops, albeit smaller in size, thereby increasing the albedo of clouds in the Earth's atmosphere; and
- 3) indirect effects of aerosols on heterogeneous atmospheric chemistry .

The first two of these mechanisms will be discussed below, following a discussion of sources of tropospheric aerosol in the Earth's atmosphere.

8.2.3.1 *Natural emission of tropospheric aerosols*

Volcanoes can be major local contributors to tropospheric aerosols, particular as a consequence of basaltic activity of long duration (months to years). Benjamin Franklin is usually credited with first making the association between a volcanic eruption and climate or weather. While he was U.S. Ambassador to France in 1783, he theorized (in an article published in 1784) that the awful haze or dry fog, presumably sulfuric acid aerosols, that hung over Paris in the latter part of 1783 was caused by an eruption in Iceland. In fact, one of the world's greatest historic lava-producing eruptions was happening at Laki, Iceland, from June 1783 to February 1784. In this event, most of the aerosols generated may have been limited to the troposphere; this is a good example of an eruption of long duration maintaining tropospheric aerosols. Under this haze, as with other aerosol veils, the sun's rays were dimmed, and anomalously cold weather occurred, including bitter cold in August and the coldest winter on record in New England.

Biological processes are an important source of aerosols. Particulates of biological origin are derived from living organisms, such as protein-containing cells, microorganisms, and fragments of living things (Jaenicke 1993). This includes a wide range of biogenic particles, such as small viruses, bacteria, algae, pollen grains, plant debris like leaf litter, and terpenes, consisting of unsaturated hydrocarbons, C₁₀H₁₆, found in essential oils and oleoresins of plants, such as conifers. Other natural sources include fires, dust from deserts, and conversion from sul-

fur-bearing biogenic emissions such as dimethyl sulfide (DMS) and sea salt. Biogenic aerosols with radii greater than 2 μm derive from plants that release pollen, spores, and terpenes into the atmosphere. Biological aerosol smaller than 2 μm in radius originate to some extent from the mechanism of bubble-bursting on the ocean surface (Blanchard and Syzdek 1972), but they are mostly produced by industrial (sewage plants), agricultural (fertilizing, etc.), or municipal activities. Hence, biological particles are derived both from natural sources and human activities, and can, under certain circumstances, have hygroscopic properties that affect the water- and ice-nucleating capacity of the atmosphere.

8.2.3.2 *Anthropogenic sources of aerosols*

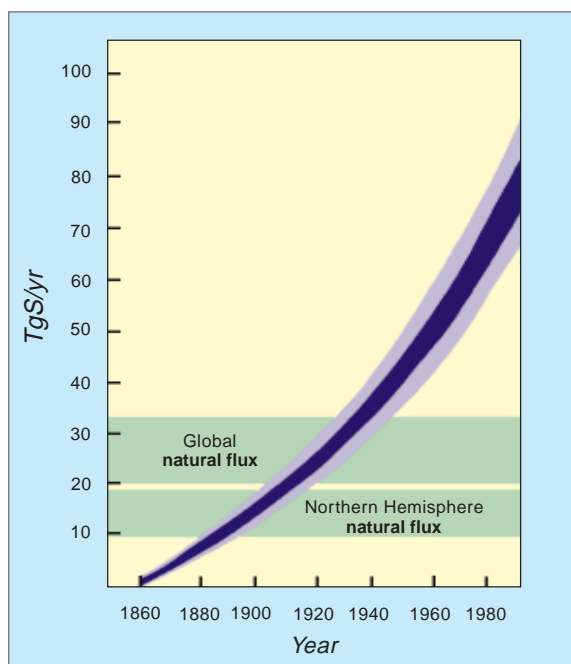
Except for increases in methane that may produce increased stratospheric water vapor, direct anthropogenic influences on stratospheric aerosols are thought to be small, although the injection of aerosols by subsonic aircraft flying in the lower stratosphere may be significant. Most of the sulfate produced by humans is converted to aerosol form in the troposphere and precipitated before it reaches the stratosphere. Stratosphere-troposphere exchange is not completely understood and the chemistry is complex, so this issue should be studied further.

The sources of aerosols associated with human activities are very important in the troposphere. Anthropogenic aerosol particles can be emitted directly (primary aerosol), or formed later in the air from oxidation of the emitted trace gases (secondary aerosol). The primary aerosols include industrial dust and soot, aircraft exhaust in the upper troposphere, automobile exhaust, particulates emitted through biomass burning, and organic particles produced in the process of biomass burning from hot unburned gases emitted from the fire and condensed immediately in the cooler air (IPCC 1995). Soil and desert dust also can be considered pseudo-anthropogenic (Prospero and Nees 1976) because of the human impact on land cover and desertification (Tucker et al. 1991). Tegen and Fung (1995) estimated the dust contribution from disturbed soils ("pseudo-anthropogenic") to be $50 \pm 20\%$ of total dust sources. Secondary aerosols include aerosol particles formed in the air from oxidation of anthropogenic SO_2 , NO_x , or volatile organic carbon (VOC). The oxidation can take place in the air or in clouds. These trace gases are also emitted from coal and oil burning in industrial or urban activities or automobile or aircraft exhaust emissions. VOC is emitted from evaporating organic compounds such as gasoline and industrial organic materials.

The effects of aerosol particles on radiative forcing (e.g., by reflecting sunlight to space), on the radiances measured from satellite sensors, on cloud formation, and on heterogeneous chemistry depend in part on their size distribution. The smaller the particles, the larger the number of particles formed for the same aerosol mass. Optically, the most effective particles are 0.2-0.8 μm in diameter. For smaller or larger particles, the particles scatter less visible radiation per unit mass. The particle size and properties are controlled by the production process. There are three main types of such processes: mechanical grinding producing mainly micrometer-size particles, gas-to-particle conversion (both oxidation and condensation) producing submicrometer particles, and production of black carbon (soot) as the unburned carbon remnant in combustion processes. Soot is emitted as very small particles ($<0.1 \mu\text{m}$), serving as condensation centers to other particles (organic particles from biomass burning), or forming chains and collapsing into round submicrometer aggregates in the presence of high humidity.

Based on the latest report of the Intergovernmental Panel on Climate Change (Intergovernmental Panel on Climate Change [IPCC] 1995), if we exclude the anthropogenic impact on soil and desert dust, the contribution of anthropogenic sources to micrometer-size particles is very small (5% of total mass). The contribution to submicrometer particles is large (~75%): sulfates - 140 Tg/yr (with a range between 120 and 180), organic particles from biomass burning - 80 Tg/yr (between 50 and 140), and VOC - 10 Tg/yr (between 5 and 25); this is out of a total budget of submicrometer particles from anthropogenic and natural sources of 390 Tg/yr ($\text{Tg} = 10^{12} \text{g}$). Soil dust also contributes to the population of submicrometer aerosols. Tegen and Fung (1995) estimate that disturbed soils contribute 50-150 Tg/yr of submicrometer particles. These numbers indicate that human activity controls the atmospheric concentration of submicrometer particles, and with that it probably influences the microphysical properties of clouds everywhere except at locations remote from human influence. The volume size distribution of most of these submicrometer aerosol types is in a size range with a large scattering cross section per unit volume. For sulfates, the volume distribution is between 0.1 and 0.4 μm in diameter (Hoppel et al. 1990; Hegg et al. 1993, 1995; Kaufman and Holben 1995) and for smoke between 0.2 and 0.4 μm (Andreae et al. 1988, 1994; Artaxo et al. 1994; Kaufman and Holben 1995). It follows from this discussion that sulfates and biomass burning are the two most significant anthropogenic sources of aerosol that can affect climate. For the same reason, these are the two types of aerosol that are

FIGURE 8.5



Time history of global emission of SO_2 (in Tg/yr) and estimates of the global and Northern Hemisphere natural flux (Charlson et al. 1992). Anthropogenic sulphur is emitted mainly (90%) in the Northern Hemisphere, and emissions greatly exceed the natural emissions. Width of shading represents the uncertainty.

the easiest to observe from space, due to their high scattering and backscattering efficiency. There is a remaining uncertainty in the anthropogenic component of soil dust, and in the role of VOC in controlling the number of cloud condensation nuclei (CCN). Though the rate of emission of VOCs is only one-eighth that of sulfates, due to their smaller size (less than $0.1 \mu\text{m}$) they may contribute as many CCN as sulfates (Rivera-Carpio et al. 1995) or even dominate the CCN concentration (Novakov and Penner 1993). The effect of aerosol on CCN and cloud microphysics is non-linear (Leaitch et al. 1986); therefore, a large concentration of VOCs can have a substantial effect on clouds but also decrease the influence of sulfates on clouds as well. The subject of aerosol-cloud interactions has been reviewed by Hobbs (1993).

8.2.3.2.1 Sulfur emission and oxidation to sulfate particles

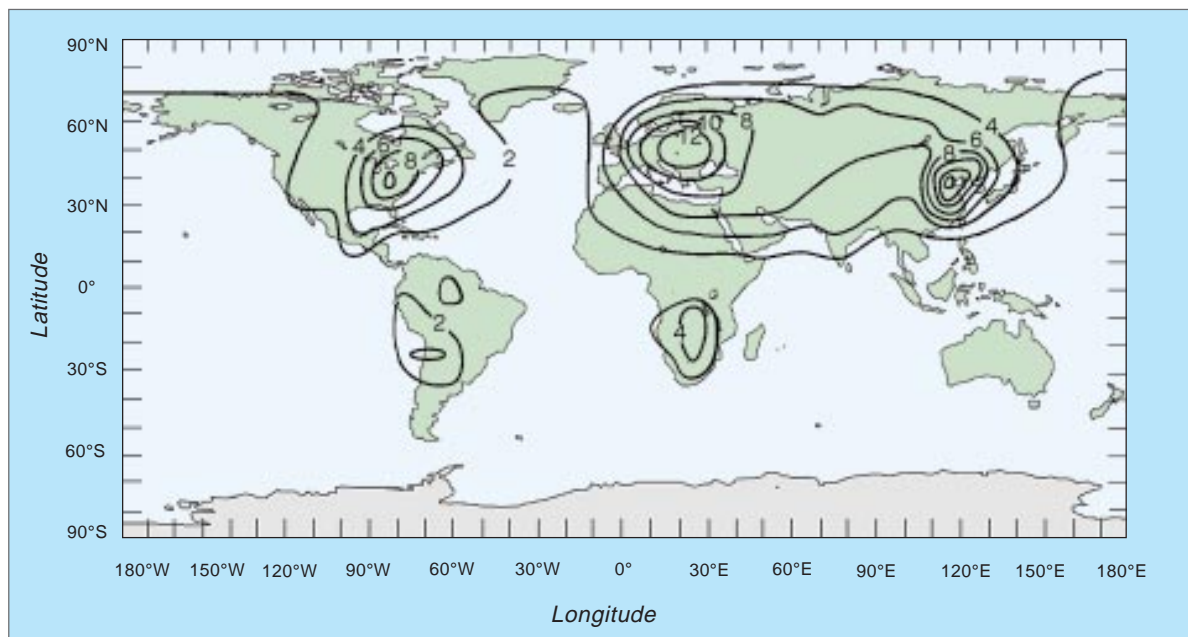
Most sulfur emission (in the form of SO_2) originates from the burning of fossil fuel (coal and oil) in the Northern Hemisphere. Muller (1992) estimated the strength and geographical distribution of the sources and the total source strength. Charlson et al. (1992) compared the total

anthropogenic sulfur budget in the last century, based on Muller's estimate, to the natural emissions (Figure 8.5). Volcanoes can make large short-term, localized contributions to the global inventory of SO_2 (Spiro et al. 1992). About half of the sulfur is deposited directly on the ground and half is oxidized in the atmosphere to form aerosol particles. Langner and Rodhe (1991) used a GCM with sulfur chemistry to simulate the transport and oxidation of the emitted anthropogenic SO_2 into aerosol particles, showing contour lines of concentrations of the particles. Figure 8.6 (pg. 352) reproduces their results. The model includes the two paths of oxidation into sulfate particles. Gas phase oxidation controls the population of particles smaller than $0.1 \mu\text{m}$, and oxidation in non-precipitating clouds controls the concentration of larger particles (~ 0.2 to $0.4\text{-}\mu\text{m}$ diameter, Hoppel et al. 1990). Langner et al. (1993) calculated with their GCM model that 88% of the anthropogenic sulfate is generated in clouds, while 12% is generated in the gas phase. The balance between these two processes and the value of maximum supersaturation reached in clouds is critical to the determination of the effect of sulfate on climate. While conversion of sulfate into larger particles in cloud processes increases their direct radiative forcing (Lelieveld and Heintzenberg 1992), it decreases the concentration of potential CCN by generating larger and fewer particles for the same sulfate mass concentration. This balance depends not only on the value of the maximum supersaturation reached in clouds, a measure that is highly unknown, but also on the variability in this value between non-precipitating clouds (Kaufman and Tanré 1994).

8.2.3.2.2 Biomass burning

Biomass burning is widespread, especially in the tropics, where $\sim 80\%$ of biomass burning takes place. It serves to clear land for shifting cultivation, to convert forest to agricultural and pasture land, and to burn dry vegetation to fertilize the soil. Biomass burning is also used for cooking and charcoal production mainly in the developing countries. Interest in biomass burning started when it was discovered to be a main missing source of greenhouse trace gases in the 1970s (Crutzen et al. 1979). It was later recognized as an important source of aerosol particles (Radke et al. 1991; IPCC 1995) that can affect clouds and the hydrologic cycle in the tropics (Crutzen and Andreae 1990) and solar radiation and climate (Penner et al. 1992). The type of aerosol produced in the burning depends on the fire temperature and oxygen supply. Hot flaming fires, typical of grassland fires in Africa and South America, produce a relatively small amount of organic particles, but a large amount of black carbon (Cachier et al. 1989;

FIGURE 8.6



Calculated distribution of the vertically-integrated amount of sulphate aerosol due to anthropogenic emissions only (Langner and Rodhe 1991: slow oxidation case). Values are annual averages expressed as mg sulphate per square meter and the maxima are associated with main industrialized regions. No comparable results are available for aerosol from biomass combustion.

Ward et al. 1992). Deforestation and other fires with a long smoldering phase produce little black carbon and a large amount of organic particles (Ward and Hardy 1991). In the last century the rate of biomass burning has increased substantially. Deforestation was almost nonexistent in the last century and now consumes 1300 Tg of carbon in biomass per year (Andreae 1995). Domestic use of biomass as fuel, and biomass burning associated with agriculture, probably increased proportional to the population expansion. Shifting agriculture consumes about 1500 ± 500 Tg of carbon per year, and grass fires an additional 1200 ± 800 Tg (Crutzen and Andreae 1990). These sources can emit a similar amount of organic particles as deforestation, and dominate the emission of black carbon. Detailed geographical estimates of biomass burning are given by Hao et al. (1990). But, in contrast to sulfate aerosols, evaluation of the global emission and distribution of smoke aerosols is still not available. The total estimate of biomass burning aerosol flux of 80 Tg/yr (IPCC 1995) corresponds roughly to 2% of the burned carbon or 1% of the burned biomass (Ward et al. 1992). The recently completed field phase of the Smoke Cloud and Radiation-Brazil (SCAR-B) study

should yield much new information on the properties of smoke particles from tropical biomass burning and their effects on the atmosphere.

8.2.3.3 Direct radiative effects of tropospheric aerosols

The direct effect of aerosols on the radiative forcing of climate is far more complex for tropospheric aerosols than for stratospheric aerosols, due to the wider range of chemical compositions, time and spatial distributions, range of particle sizes and shapes, interactions with water vapor and clouds, and overall global variability that is dependent on both natural sources of aerosols and human activities. In principle, the direct radiative forcing (both shortwave and longwave) by tropospheric aerosols can be computed if the optical properties of the aerosols are known, especially the spectral optical thickness, single-scattering albedo, and phase function, all of which depend on the size distribution and refractive index of the aerosols. Many of these optical and microphysical properties depend on the individual chemical species comprising the aerosols (e.g., sulfates, nitrates, silicates, sea salt, soot, organics, etc.).

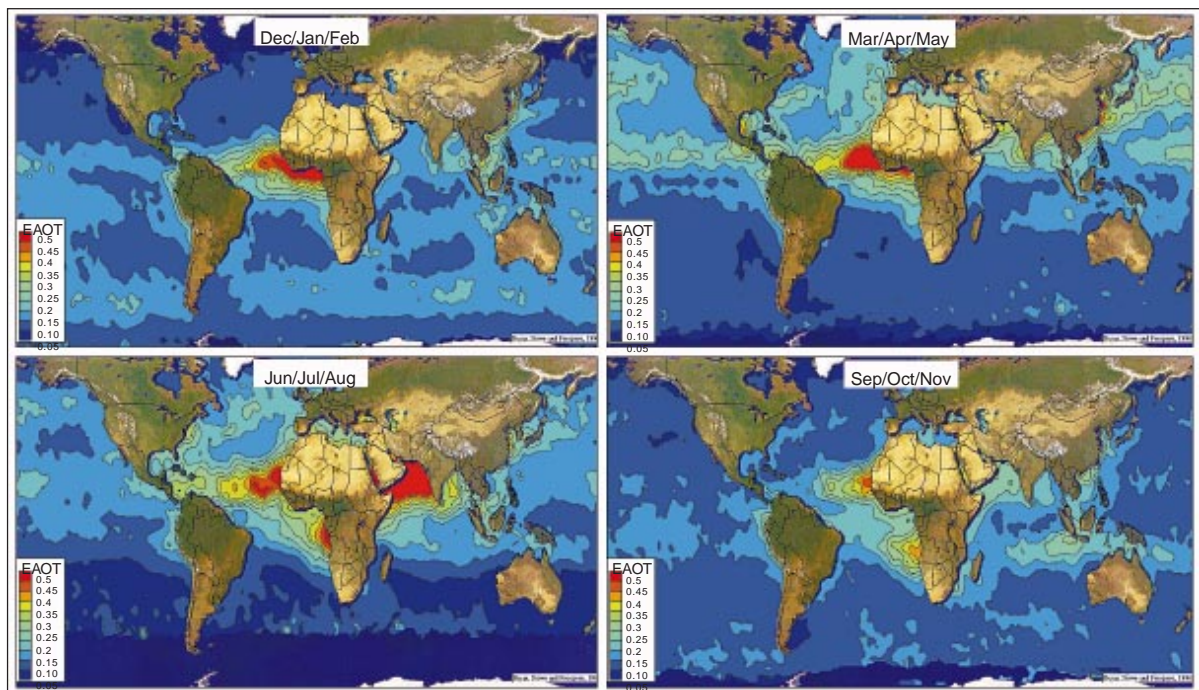
Unfortunately, reliable laboratory measurements of refractive indices of atmospheric aerosols are not available for most of the chemical species composing the atmospheric aerosol. Furthermore, since reliable particle size distributions are also incomplete, it is not currently possible to calculate with high accuracy the radiative forcing by tropospheric aerosols. This has led the scientific community to advocate the simultaneous acquisition of satellite-based radiance measurements, ground-based measurements of atmospheric transmission and sky radiance, and in situ measurements of aerosol optical and microphysical properties from aircraft. In these so-called “closure” experiments, it should be possible to verify that optical thicknesses and other radiative parameters retrieved from available satellite measurements, when inserted into a radiative transfer model, yield accurate estimates of the radiative forcing of tropospheric aerosols. The first comprehensive closure experiment was carried out in the Tropospheric Aerosol Radiative Forcing Observational Experiment (TARFOX) on the United States East Coast in the summer of 1996 (Stowe et al. 1995).

Since changes in column-integrated radiances are weakly dependent on aerosol properties, making reliable

retrieval of these properties difficult, improvements in measurement capability from current satellite systems are highly desirable to further advance our understanding of the role of tropospheric aerosols on climate. Advances from current systems are planned for the EOS missions through the use of improved radiometric accuracy and calibration (the Moderate Resolution Imaging Spectroradiometer [MODIS], the Multi-angle Imaging Spectro-Radiometer [MISR]), multi-wavelength capability over a wider spectral range (MODIS, MISR, OMI), multi-angle looks at the same scene (MISR, the Earth Observing Scanning Polarimeter [EOSP]), and multispectral polarimetric techniques to enable refractive index and characteristic aerosol types to be identified (EOSP). A necessary component of improving the determination of tropospheric aerosol properties from space is a ground-based sunphotometer and sky radiance network.

To assess the radiative forcing of industrial aerosols, it is necessary to establish the preindustrial global background aerosol with the same degree of reliability that the preindustrial greenhouse gas levels are known. Based on aerosol measurements in remote locations (e.g., Cape Grim, Tasmania, and Mauna Loa Observatory, U.S.), the global mean preindustrial aerosol optical thickness

FIGURE 8.7



Aerosol abundance over the oceans estimated from satellites (Husar, Stowe, and Prospero 1996).

may have been in the range $0.02 \leq \tau_a \leq 0.05$. Andreae (1995) estimated that the global average natural aerosol background is $\tau_a = 0.07$.

The single-scattering albedo of desert dust is largely unknown, and this aerosol type is a dominant feature of global aerosol measurements over the ocean as obtained from space (Figure 8.7). For radiative transfer purposes, the precise form of the aerosol size distribution is not important, but rather the optical thickness and effective radius (Lacis and Mishchenko 1995). Typically, in models that calculate aerosol forcing of climate, aerosol types and sizes are described by a finite number of discrete categories, with optical thickness and vertical distribution as free parameters. Consistency is needed between those aerosol parameters used in radiative transfer models and those in field measurements, where a continuum of particle sizes and composition mixtures is encountered. Closure experiments will further enhance our confidence in this transformation.

8.2.3.4 *Indirect effects of aerosols on cloud abundance, lifetime, and optical properties*

The indirect effect of aerosols refers to their effects on cloud properties: droplet/ice particle number concentrations and sizes, water/ice amounts, cloud lifetime, and cloud boundaries. Through their influence on these properties, aerosols have an indirect effect on the Earth's radiative energy balance through the way that clouds affect the Earth's energy budget. The indirect effect is often referred to as the Twomey effect. Twomey (1977) first outlined the potential role of aerosols on cloud droplets and cloud radiative properties.

The subset of tropospheric aerosols that act as the nuclei for cloud droplet formation is known as cloud condensation nuclei (CCN). These nuclei serve as seeds around which water condenses to form droplets and ice crystals. Increased numbers of CCN are correlated with increased numbers of cloud hydrometeors (Warner and Twomey 1967; Martin et al. 1994). Often, however, the new droplets compete for the water that is available for condensation so that while increased CCN lead to increased numbers of hydrometeors, the size of the hydrometeors is smaller (Twomey 1977; Radke et al. 1989; King et al. 1993; Garrett and Hobbs 1995). Because scattering is proportional to the surface area of the scattering targets, a given mass of water scatters more light if it is distributed among smaller particles. Consequently, polluted clouds are expected to have higher reflectivities than their non-polluted counterparts. Satellite and aircraft observations have confirmed this increase in reflectivity (Coakley et al. 1987; Radke et al. 1989;

King et al. 1995). This increase is expected despite the absorption of sunlight by the aerosol, although if the optical thickness of the cloud and the absorption of sunlight by the aerosol are sufficient, the effect of the absorption can lead to a decrease in cloud reflectivity despite the increase in droplet number (Twomey 1977). This decrease has also been confirmed through satellite observations of the effects of biomass burning on cloud radiative properties (Kaufman and Nakajima 1993).

Through their influence on droplet and ice particle numbers and sizes, aerosols may influence bulk cloud properties, such as cloud amount, lifetime, cloud liquid/ice water amounts, and the locations of cloud boundaries. Clouds with large numbers of small droplets appear to show smaller occurrences of drizzle than do their counterparts having relatively few but large droplets. Consequently, clouds affected by increased aerosol burdens are expected to retain cloud water while unaffected clouds are expected to lose their water. Affected clouds have been predicted to last longer in the atmosphere than their unaffected counterparts (Albrecht 1989). The added lifetime could give rise to larger cloud cover fractions when averaged over time (Parungo et al. 1994; but see Norris and Leovy 1995). Results from the recently completed Monterey Area Ship Track Experiment show that these expectations are not always realized.

If one is to believe some of the simpler models for cloud properties, such as mixed-layer models for marine stratus, then hydrometeor size, through its influence on radiative heating, affects the thermodynamic environment of the cloud thereby influencing the location of the cloud boundaries (Pincus and Baker 1994). Such changes, however, are expected to be small, making them difficult to detect.

Because the evolution of aerosol precursors to CCN and ultimately to cloud droplets is fraught with uncertainty, assessments of the indirect effect are also fraught with uncertainty. The range of possibilities seems limitless (Kaufman et al. 1991) but may well be of the same order of magnitude as that due to the direct effect (Charlson et al. 1992). One obstacle to reducing the uncertainty is lack of knowledge linking precursor gases to the existing levels of CCN. What fraction of the precursor gases gives rise to new particles and new hydrometeors and what fraction is absorbed by existing particles and hydrometeors? For example, a major fraction of the SO_2 emitted into the atmosphere appears to be taken up by existing cloud droplets rather than giving rise to new particles (Langner et al. 1992).

The relationship between the number of particles and the number of cloud droplets appears to saturate at

high aerosol concentrations (Leaitch et al. 1992; Martin et al. 1994). Clouds can have such a large population of small droplets that adding new particles to the cloud has little if any effect on the droplet size distribution. Nevertheless, substantial changes have been observed, even for continental clouds with their large number concentrations and small droplet sizes (Braham 1974). Also, the effect of a transformation of droplet size on cloud radiative properties becomes saturated when the number of droplets is large and thus cloud reflectivities approach their upper limits (Charlson et al. 1992; Platnick and Twomey 1994).

8.2.3.5 *Science investigations using EOS data*

EOS aerosol data products will be used to study variations in the anthropogenic aerosol, its interactions in the atmosphere, and its radiative forcing of climate. Some of the research is planned by EOS investigators; other research will be done outside of EOS using EOS data. EOS data will be used to monitor the change in the aerosol global loading. Using global transport models that include atmospheric heterogeneous chemistry (e.g., Benkovitz et al. 1994), it should be possible to investigate to what degree changes in aerosol concentrations are due to changes in the source strength and redistribution of the location of the sources (e.g., reduction of emission in some areas and an increase in others) or due to changes in the rate of atmospheric processes that affect aerosol properties and sinks. Comparison between simultaneously-derived EOS aerosol concentration and properties with cloud abundance and properties (King et al. 1992) will be used to study the effect of aerosol on cloud droplet size, cloud reflectance, and maybe even cloud cover (Twomey 1977; Twomey et al. 1984; Coakley et al. 1987; Radke et al. 1989; Kaufman and Nakajima 1993; King et al. 1993). The aerosol distribution and properties will also be used to correct satellite observations of the land and ocean surface for aerosol effects (atmospheric correction).

8.2.3.6 *Needed satellite and in situ measurements*

Learning how aerosols affect the global climate requires: 1) The space-based monitoring of indices related to aerosol properties; 2) surface-based monitoring of indices related to aerosol properties; and 3) intensive field campaigns. The surface-based monitoring program should be designed to enhance the capabilities of the space-based program. Because the inference of aerosol properties from space is an ill-posed problem, a surface-based monitoring program is crucial to the success of the space-based program. The surface-based program will not only track the performance of space-based monitoring, it could provide additional information concerning the aerosol

properties for a number of major aerosol systems (maritime, urban, windblown dust, volcanic, biomass burning, etc.) that enhance the interpretation of the spaceborne observations. Field campaigns, in turn, are designed to refine knowledge gained from both the surface and space-based monitoring programs. The emphasis of the field campaigns will be to learn how aerosol properties are linked to sources and sinks, and how these properties are transformed by atmospheric processes. The links between aerosol properties and aerosol sources and sinks are essential to assessing the influence of aerosols on the climate system.

8.2.3.6.1 *Global observations of tropospheric aerosol optical properties*

The direct effect of aerosols can be observed from space through their effects on the scattering and absorption of sunlight. Since most aerosols have sizes in the 0.1-1.0 μm range, their effect on escaping longwave radiation is relatively small compared with their effect on sunlight. Aerosol properties are inferred primarily from reflectivities measured from cloud-free regions (Hansen and Travis 1974; Kaufman et al. 1990; King et al. 1992; Diner et al. 1988; Martonchik and Diner 1992; Tanré et al. 1995; Torres et al. 1998). Such strategies will be used to extract aerosol properties from MODIS, MISR, and OMI. The properties will thus be clearly limited to cloud-free conditions. While such conditions obviously bias the ensemble of observations, the ensemble is likely to remain stable over long periods and thus provide a useful index for monitoring change (Rao et al. 1989; Kaufman and Nakajima 1993).

The amount of sunlight reflected from the Earth system is a function of aerosol burden and aerosol properties such as particle size and single-scattering albedo. Short-term variations in reflected sunlight at visible wavelengths within cloud-free regions are linked to short-term variations in the column aerosol burden. Reflected sunlight in the near infrared ($>1 \mu\text{m}$) is expected to provide an index of particle size (small vs. large, with $r \sim 0.7 \mu\text{m}$ being the approximate size partition [Durkee et al. 1986]). This index helps characterize the aerosol and may ultimately help identify the source of the aerosol: urban, maritime, or windblown dust. Contrasts in reflected light over backgrounds with varying albedos, such as contrasts between small lakes and their surroundings, forests, and nearby grasslands, etc., are expected to provide an index for the single-scattering albedo (Kaufman 1978). Like particle size, such inferences will lead to better characterization of the aerosol and help with the identification of sources. Finally, since aerosols have sizes that are com-

parable to the wavelengths of incident sunlight, their presence changes the color of the Earth. Narrowband estimates of albedo changes due to aerosols will probably be biased. Broadband observations are needed to provide unbiased estimates of the effect of the aerosol on the Earth's albedo.

Because most of the light reflected from the cloud-free Earth is reflected by the surface, inferring aerosol properties from space poses substantial signal-to-noise problems, particularly when the aerosol concentrations are low, as they are far from sources, such as urban environments, deserts, etc. Nevertheless, over oceans, monitoring of aerosol burdens comparable to those expected from the natural background (optical thickness, τ_a [0.5 μm] \sim 0.05) seems feasible (Rao et al. 1989). Similar capabilities may be achievable over dark, continental targets such as lakes and forests (King et al. 1992; Holben et al. 1992; Martonchik and Diner 1992). This will be a new challenge for EOS, with no previous experience on a global basis to determine the possible degree of success.

More reliable detection of aerosols over land is possible using near-ultraviolet wavelengths (380-400 nm) where the non-snow covered terrestrial surfaces become very dark (Eck et al. 1987; Herman & Celarier 1997). The large molecular (Rayleigh) scattering at these wavelengths has both advantages and disadvantages over the visible techniques. While it reduces the dependence of backscattered radiances on surface reflectivity and aerosol phase function, it makes them more sensitive to aerosol absorption, except when aerosols are close to the surface. Therefore, the technique is most useful for estimation of aerosol optical thickness near their source regions over land. It works particularly well in arid and semi-arid areas, where the visible techniques become unreliable.

Another UV technique developed recently (Krotov et al. 1997; Torres et al. 1998) using TOMS data is sensitive only to highly UV absorbing aerosols (volcanic ash, smoke, and mineral dust) and is insensitive to other aerosol types as well as clouds. The technique has the advantage that it works equally well over both land and water, and is the only known (passive) technique that can detect such aerosols over very bright scenes, including snow and underlying clouds. However, the technique suffers from strong sensitivity to aerosol height- the lower the height the less sensitive the technique. Its primary advantage is to help in the identification of aerosols detected by more conventional techniques.

Several EOS instruments will provide information about tropospheric aerosols. This includes three primary instruments designed for aerosol research (MODIS, MISR and EOSP). In addition, the OMI instrument on EOS/

CHEM, which has UV channels, would provide aerosol information similar to TOMS, and the GLAS lidar in ICESat will provide aerosol backscattering profiles.

MODIS, which will fly on both the EOS AM-1 and PM-1 platforms, will make reflected spectral measurements in the solar and infrared regions to obtain aerosol optical thickness. Over ocean it will also provide aerosol size distribution, namely the ratio of the concentration of micrometer to submicrometer particles, and the specific size of the dominant aerosol mode. Over land the information will be initially limited to the determination of whether the dominant mode is of micrometer or submicrometer size (King et al. 1992; Tanre et al. 1995). However, combination of MODIS with TOMS and OMI has the potential of improving the size information over land, as well as helping in the identification of aerosol types over both land and oceans.

MISR, which will fly on EOS AM-1, will make multi-angle measurements at four visible and near-infrared bands (Diner et al. 1998, 1991). The angular and spectral measurements will be used to derive the aerosol optical thickness and loading over land and ocean. With the help of an aerosol climatology to remove some of the indeterminacy of the aerosol properties from space observations, the MISR aerosol retrieval should be able to distinguish among many common particle "types" that represent constraints on a combination of particle shape, size distribution, and composition.

Combining spectral measurements in the solar spectrum with polarization measurements, to be obtained with EOSP, provides additional information on aerosol properties. EOSP may fly on an EOS AM-2 platform, along with advanced versions of MODIS and MISR. The addition of polarization measurements is expected to refine the EOS ability to measure the size distribution of the climatically-important small particles, and to help in establishing the aerosol refractive index, a parameter that is both important for the inversion of satellite-measured radiances to aerosol properties, and for illuminating the chemical composition and atmospheric influences on aerosol particles.

Again, the direct effect of aerosols can be extracted only for cloud-free conditions. Further, they are often seen as a small residual viewed against the noisy cloud-free background offered by the Earth's surface. In order to assure that global-scale aerosol systems are being fairly represented in the combination of space and surface-based monitoring, occasional surveys with spaceborne lidars, as recently undertaken by LITE, should be performed (McCormick et al. 1993). LITE frequently found aerosol systems, like smoke above extensive marine stratocumu-

lus layers to the west of South America, that may well be missed by conventional passive techniques being planned for aerosol monitoring. GLAS, to be launched in 2001 on the Ice, Clouds, and land Elevation Satellite-1 (ICESat-1), will provide a similar global capability of monitoring the vertical profile of aerosol layers in the troposphere and lower stratosphere. This will be especially important in polar regions, where multilayer cloud and aerosol systems are common and for which passive imaging systems are less capable.

The ability to differentiate tropospheric aerosols from stratospheric volcanic aerosol layers is clearly desirable. Techniques that rely on the intensity of reflected light to gain aerosol properties, such as those that will be employed with MODIS and MISR observations, cannot separate light reflected from the troposphere from that reflected from the stratosphere. Limb observations, such as those employed with SAGE III, are essential to accounting for the light reflected from volcanic haze layers (McCormick and Wang 1987). While observations of the polarization of reflected light might be used to infer indices of the vertical distribution of aerosol properties, it is doubtful that such indices can compete with the integrity of the solar occultation provided by the limb observations. Once accounted for, residual contributions to reflected light for cloud-free regions can then be used to infer the properties of tropospheric aerosols. So, limb viewing instruments such as SAGE III are crucial components to an aerosol monitoring program.

Once global distributions of aerosols are derived on a daily basis, they can be used with global models (Benkovitz et al. 1994; Langner and Rodhe 1991) to derive aerosol fluxes, calculate aerosol nonaqueous mass, determine their sources and sinks, and compute their radiative forcing effect on clouds and the hydrological cycle, and the effect of aerosols in atmospheric chemical processes.

The effect of aerosols on clouds is best manifested through changes in hydrometeor size, which in turn is best detected through changes in reflected sunlight at near-infrared wavelengths (King et al. 1992). Water and ice absorb in the near infrared. To a first approximation, the absorption cross sections of water droplets and ice particles are proportional to the particle volume, while the scattering cross sections are proportional to the particle area. The ratio of scattering to absorption thus becomes a sensitive function of particle size in the near infrared. The ratio of scattering to absorption is, in turn, linked to cloud reflectivity.

While upper-level clouds have often been characterized as having ice crystals with sizes ranging from

10-100 μm , evidence from multispectral emission in the infrared (Prabhakara et al. 1988; Lin and Coakley 1993) and from in situ observations (Strom 1993) suggests the presence of smaller particles for upper-level clouds. Such particles should also manifest their presence through their effect on reflected sunlight in the near infrared.

Links between cloud hydrometeor sizes and bulk properties of clouds such as cloud lifetime, cloud top altitude, cloud thickness, and liquid water content, could greatly alter the ways in which aerosols affect the Earth's radiation budget. Such links are anticipated, but evidence for these links will come only from careful long-term monitoring of cloud systems. The cloud properties that must be monitored are hydrometeor size, amounts of water and ice, the vertical extent of the cloud, and the fractional cloud cover of the cloud systems. Since all of these properties affect the way in which clouds affect the Earth's energy budget, these properties are expected to be monitored in any case (King et al. 1992). The monitoring, however, should be so extensive as to allow a study of large-scale cloud systems that are transected by aerosol systems so that one portion of the cloud system has a high probability of being affected by aerosols and a second portion has a low probability of being affected. Cloud systems that span an urban plume and surrounding areas that lie outside of the plume would be an example. In such cases, the affected and unaffected portions of the cloud system can be examined together. They would be expected to be very similar except for the effects of the aerosol. With extensive monitoring, ensembles for particular types of cloud systems can be built and studied for the effects of the perturbing aerosols.

8.2.3.6.2 Surface monitoring of tropospheric aerosols

Surface-based monitoring should be designed to improve space-based capabilities, since satellite measurements alone cannot detect all aerosol properties. Some aerosol properties must be pre-assumed, based on previous measurements, and/or measured in parallel with space observations (Wang and Gordon 1995). Because they will be used to track the performance of the spaceborne monitoring capability, the surface-based observations must be reliable. Sites for the surface-based observations should be distributed in order to characterize some of the well-known aerosol systems: urban haze, desert dust, smoke from biomass burning, etc. The observations should include measurements of radiation along with surface measurements of the physical and chemical properties of the aerosol. The coupling between radiation and physical and chemical properties of aerosols will lead to better estimates of the effect of aerosols on the Earth's radiative

energy budget. Furthermore, the inclusion of observing capabilities for the physical and chemical properties will help link aerosol properties to their sources and sinks (Charlson et al. 1992).

EOS, together with other international Earth science organizations, is planning a network of ground-based automatic instruments that will remotely sense aerosol properties from the surface (Holben et al. 1995). The ability to observe both the sun through the aerosol layer as well as aerosol scattering relative to the dark background of space (sky radiation), makes these ground-based remote-sensing measurements very powerful (Nakajima et al. 1989; Kaufman et al. 1994). Therefore, the EOS strategy is to complement the global distribution of aerosol properties derived from Earth-orbiting satellites on a daily or twice daily basis with ground-based measurements at ~100 stations worldwide. These observations should provide measurements of the diurnal cycle of aerosol concentration and optical properties, as well as supply statistics on some of the missing optical properties needed to analyze the spaceborne data. Other aerosol properties will be derived from chemical measurements and sampling by scientists worldwide.

In addition to the surface sunphotometer/sky radiance network, the surface sites should also include calibrated broadband radiometers. Simultaneous observations of multispectral radiances at the Earth's surface and from space for cloud-free conditions will enhance the ability to detect the absorption of sunlight that is otherwise difficult to infer from either surface or space-based observations alone.

8.2.3.6.3 Intensive field campaigns

To complement the surface and space-based observations of tropospheric aerosols, it is necessary to conduct periodic airborne intensive field campaigns. The roles of these campaigns include: 1) Intercalibration of spectral, angular, and polarimetric sensors on aircraft with their spaceborne counterparts; 2) in situ measurement of the optical and microphysical properties of the atmospheric aerosol, especially, aerosol size distribution and, where possible, the single-scattering albedo; and 3) providing an opportunity to confirm a closure of radiative transfer models of the transmission, reflection, and absorption of the Earth-atmosphere system with nearly simultaneous surface and spaceborne observations of sky radiance, aerosol properties, and radiative flux. These aperiodic campaigns should be carefully coordinated with the international scientific community, and should focus on particularly important aerosol climatological regimes (e.g., sulfate aerosol from the east coast of the U.S. and China, biomass burning aerosol in the tropics, Sahelian dust out-

breaks from Africa), as well as aerosols especially difficult to detect (Arctic haze, continental haze layers).

8.2.4 Volcanic hazards

Volcanoes represent significant hazards to people and property on the ground and in the air. Because each eruption is unique, it is challenging to develop a set of methodologies that can successfully identify and document the physical processes associated with all types of volcanic eruptions. For example, subtle differences in the percentage of water vapor vs. ash in an eruption plume, perhaps by interaction between the lava and surface water, can produce very different plumes that may not always be detected by thermal imagers. Ground deformation associated with swelling or subsidence of a volcano may not be accurately determined via radar interferometry due to decorrelation of the surface between observations, or due to atmospheric effects associated with the water vapor content of the atmosphere. Methodologies for the remote detection of the eruption of new lava flows, or the monitoring of the thermal output of on-going eruptions are still under development. Hyperspectral measurements at mid- and thermal-infrared wavelengths are needed to redress this situation.

Studies of volcanic hazards can be divided into three main categories. Hazard prevention refers to the analysis of dormant volcanoes, which are considered to be potentially active but show no signs of eruption in the near future. Hazard preparedness refers to restless volcanoes that currently have mild activity in the form of ground deformation, gas emissions, or elevated ground temperatures. Hazard relief is needed for active volcanoes, which may currently be erupting lava flows or undergoing explosive eruptions that generate eruption plumes, pyroclastic flows, or mudflows. Hazardous volcanoes are often particularly challenging to study because they may be located in areas where local logistics, weather, and personal safety limit access. A wide range of hazards also exists. Long-lasting emissions of tropospheric gases (HCl, SO₂, and HF) have a major impact on the health of people, livestock, and agriculture downwind of a volcano. Lava flows and, more particularly, volcanically-generated mudflows (lahars) have proven to be fatal to thousands of people in this century. A new hazard, associated with the use of aircraft flight paths over volcanically-active areas such as Indonesia and the Alaskan peninsula, places tens of thousands of jet aircraft at risk every year due to the potential for unexpected encounters with an eruption plume. Other volcanic hazards exist, including the potential that flank failure will generate tidal waves (tsunamis) in shallow marine environments (e.g., St. Augustine, Alaska).

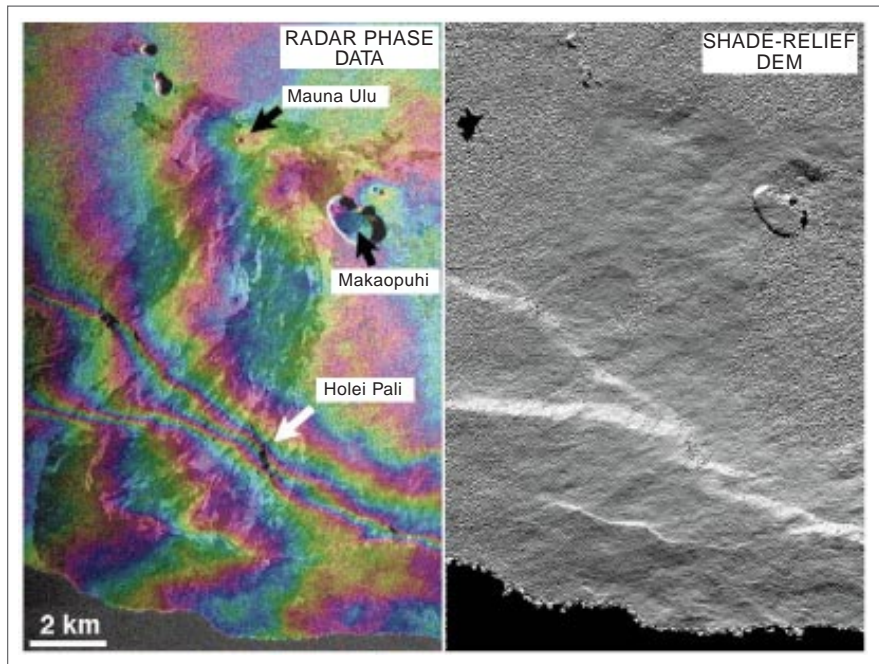
The major challenge to satellite-based observations of volcanic hazards is the development of techniques that can be used in a predictive manner to detect an evolving volcanic crisis, and to provide timely information to the relevant authorities on the ground.

8.2.4.1 Health hazards of tropospheric volcanic gases and aerosols

Basaltic volcanoes such as Kilauea, Hawaii, can be in near-continuous eruption for years (in Kilauea's case, more than 12 years). While the daily eruptions of volcanic gases (including H₂O, CO₂, SO₂, H₂, CO, HCl, HF, and H₂S) are quite low, with average emissions in the range of 1000-2000 tons/day, the protracted nature of the eruptions can place local populations at serious health risk. In a more-extreme case, the 1783 eruption of the Laki Fissure in Iceland erupted ~125 Tg of SO₂ in five months (equivalent to five Mt. Pinatubo eruptions), and caused numerous weather anomalies in Europe including dry fogs and high optical thicknesses. This eruption is also believed to have caused a drop in the global mean surface temperature of ~1-to-3°C (Sigurdsson 1990).

H₂O and H₂ can be dismissed as significant health factors, either because of their low inherent toxicity, low concentration in volcanic emissions, or both. SO₂, H₂S, and their reaction products present the greatest potential for adverse health effects, which are further magnified by their ultimate conversion in the atmosphere to a secondary acid aerosol, producing irritants with demonstrated adverse effects on the human respiratory system. HCl and HF emissions from volcanic vents, while very low relative to SO₂, also contribute to the acidic nature of the atmosphere downwind of the volcano. Both are strong irritants capable of causing lung injury.

FIGURE 8.8

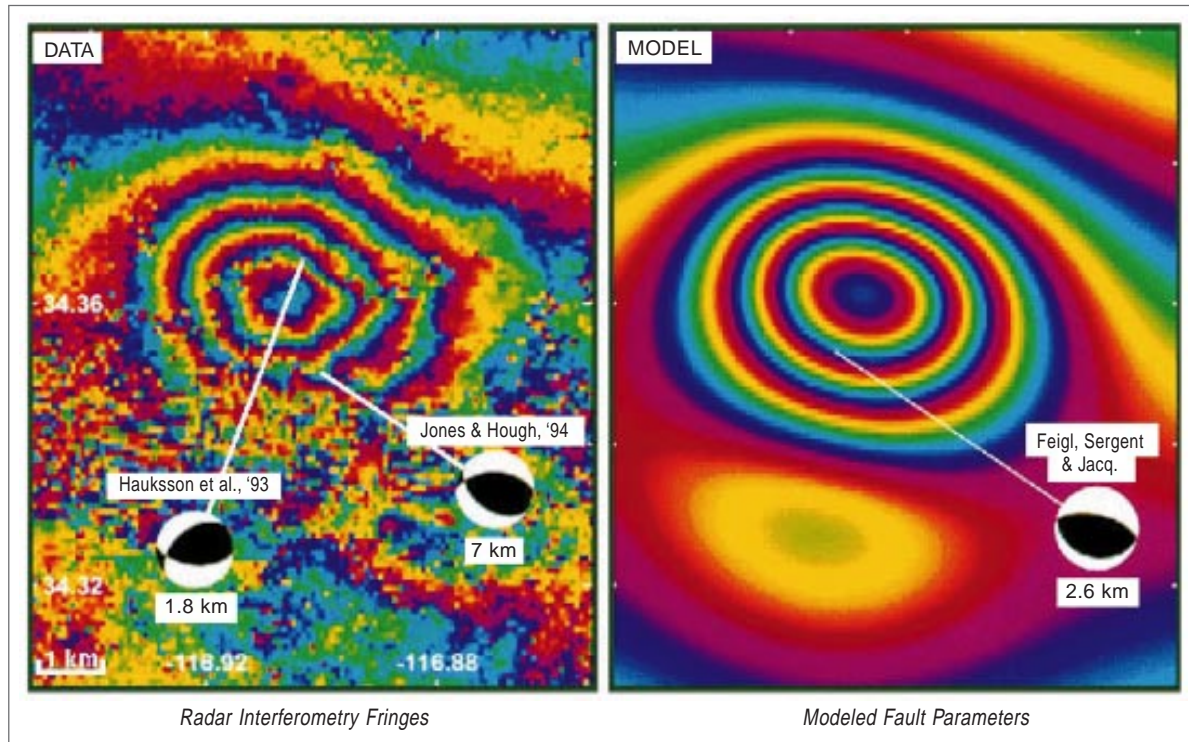


Radar interferometry will be used extensively to construct digital elevation models of volcanoes, using data from foreign-partner radars such as ENVISAT ASAR and RADARSAT. Space Shuttle Radar (SIR-C) data collected in October 1994 are used here first to construct a radar phase map (left) of the Mauna Ulu area of the Kilauea volcano in Hawaii. These phase data can then be unwrapped to generate a digital topographic map, which then can be used to produce the shaded relief map (right). Almost 1 km of relief is shown in this image, with the bright escarpment representing ~350 meters of elevation change (*unpublished data; courtesy of Harold Garbeil and Peter Mougini-Mark [University of Hawaii]*).

Sulfate concentrations in rain water due to ongoing eruptions also have a significant impact on the downwind population. Where lava flows enter the ocean, a further health hazard is generated by the production of steam clouds. In extreme cases, rain water has been found to have a pH in the range 2.4 to 2.8, and has been correlated with health problems in local populations that rely on rain for drinking water. Direct analysis of this steam plume indicates that it is an acid brine with a salinity ~2.3 times that of sea water and a pH ranging from 1.5 to 2.5!

CO₂ hazards from volcanoes should also not be forgotten. In Cameroon, the release of carbon dioxide gas from an overturned volcanic water lake resulted in hundreds of fatalities in 1986. Many deaths in the historical record are attributed to asphyxiation by volcanic gases, mostly by CO₂ and H₂S (Simkin and Siebert 1994). CO can also reach toxic levels as it did in Niragongo in 1972 (Faivre-Pierret and Le Guern 1983). The risk posed by such hazards can be assessed by means of modeling the ground flow of such gas discharges, provided that there is a high-quality digital elevation model (DEM) available.

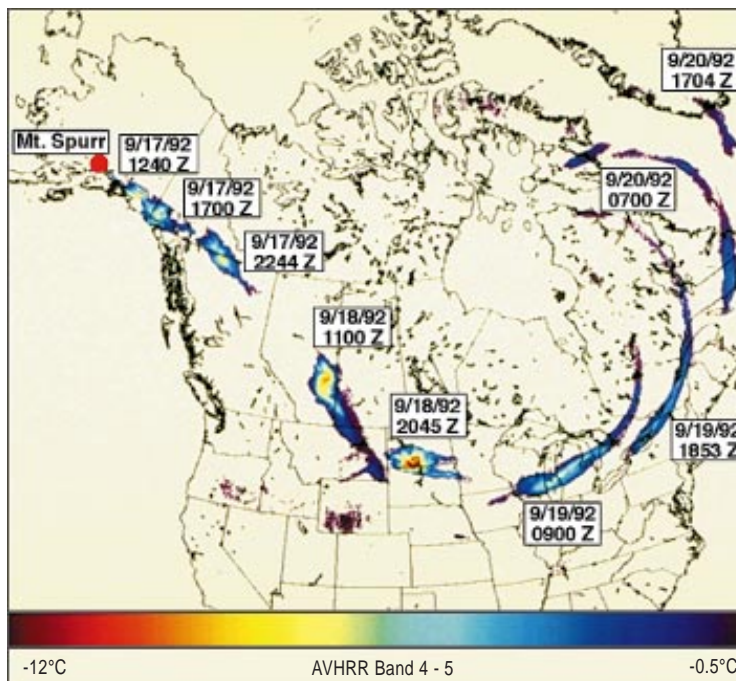
FIGURE 8.9



Fringes produced by a small ($M=5.1$) aftershock, as seen in an interferogram constructed from European Remote-Sensing Satellite-1 (ERS-1) radar images acquired on April 24, 1992 and June 18, 1993 (left: *Massonet et al., 1994*), and modeled using fault parameters estimated from the interferogram (right: *Feigl et al. 1994*). The interferometric signature is the sum of the main Landers shock (straight fringes in NE quadrant) and the aftershock (concentric circles near center). One fringe represents 28 mm of range change.

Weather satellite data are already used in an operational mode by the FAA, U.S. Geological Survey, and the Australian aviation community. These data are used to detect and track volcanic eruption clouds, which represent a great danger to air traffic along many of the world's busiest air routes. Due to the presence of silicate material in the cloud, the spectral properties of volcanic clouds and weather clouds are very different in the thermal infrared, allowing simple automatic detection algorithms to be developed in a comparable way to more-detailed analyses from MODIS. Here we see four days of coverage for the cloud from the September 17, 1992 eruption of Mt. Spurr in Alaska. This cloud was responsible for closing Chicago's O'Hare Airport for several hours, causing major problems for air traffic from Alaska to New England (*unpublished data; courtesy of Bill Rose [Michigan Technological University]*).

FIGURE 8.10



8.2.4.2 Lava flows and volcanic mud flows

Imaging radar aids the analysis of volcanoes due to its cloud-penetrating and all-weather capabilities. Radar interferometry has the potential to address all three categories of hazards through the collection of DEMs and the monitoring of centimeter-scale changes in topography (Figure 8.8). To date, Topographic Synthetic Aperture Radar (TOPSAR) DEMs have been used to assess the distribution of slopes on volcanoes (e.g., Mouginis-Mark and Garbeil 1993) and the thickness and width of lava flows as a function of distance from the vent (Evans et al. 1992). TOPSAR data could also permit hazard maps to be developed using numerical models for the emplacement of lava flows (Wadge et al. 1994) or pyroclastic flows (Malin and Sheridan 1982). Deformation studies of volcanoes are also possible using orbital radars. Analysis of the Landers earthquake (Figure 8.9) shows that changes on volcanoes undergoing tumescence (e.g., the summit of Mauna Loa, Hawaii) or erosions following eruptions (e.g., the lahars channels of Mt. Pinatubo, Philippines) can both be monitored.

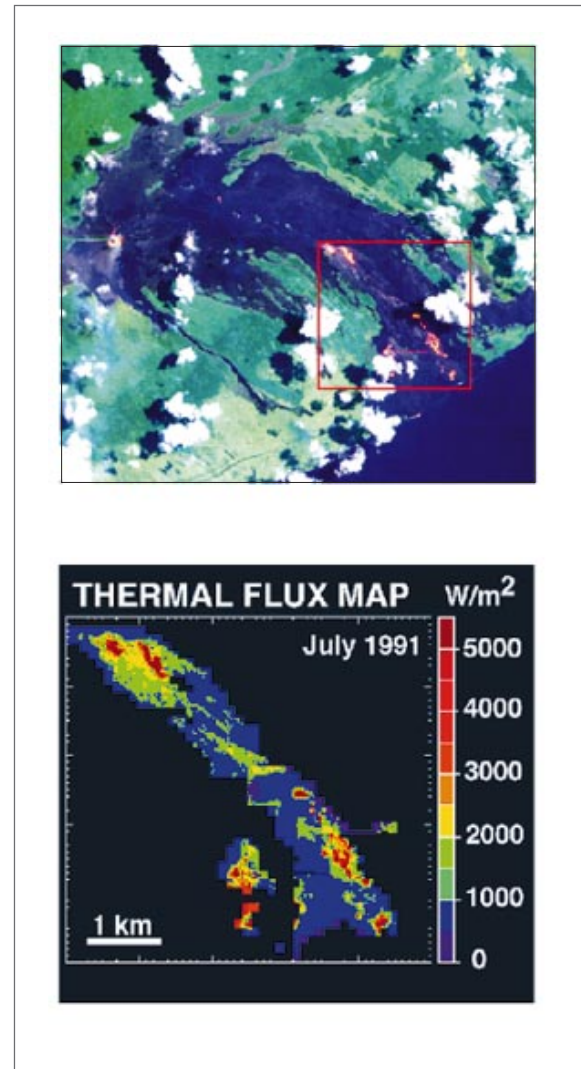
8.2.4.3 Hazards to aircraft from eruption plumes

Aircraft-ash encounters are another area of great concern. There have been several near-fatal accidents, the most spectacular being the 747 jumbo jet crippled by ash from Redoubt while entering Anchorage air space on 15 December 1989 (Brantley 1990). The Federal Aviation Administration (FAA) volcanic-ash-avoidance procedure is designed to avert future disasters from ash being ingested into aircraft engines (Casadevall 1994). Nevertheless, there is a critical need for increased surveillance of volcanoes in the context of aircraft safety, particularly over remote volcanoes along established commercial air routes (e.g., the North Pacific) (Figure 8.10).

8.2.4.4 Needed satellite and in situ measurements

The eruptions of the El Chichón (Robock and Matson 1983), Colo (Malingreau and Kaswanda 1985), Galunggung (Prata 1989), Augustine (Holasek and Rose 1991), and Redoubt (Kienle et al. 1990) volcanoes demonstrate the potential application of satellite images for detecting eruption plumes. A key factor in making future satellite observations useful for hazard assessment is the rapid identification of new eruptions under a variety of observational conditions such as time of day, viewing geometry, and solar azimuth angle. To be of value to, for instance, airlines and government agencies, a reliable technique has to be found for the automatic detection and analysis of eruption plumes using weather satellite images.

FIGURE 8.11



ASTER data will be routinely used to study the temperatures of active lava flows. Simulations of these data can be derived from Landsat Thematic Mapper data (top). Illustrated is the July 1991 eruption of the Kilauea volcano in Hawaii. While knowledge of the temperatures is important, a far more valuable data product is a map of the total thermal flux of the lava flow, since this provides information on the degree of vigor of activity and the relative age of day-old lava flows. The bottom panel shows a thermal flux map for the area shown in the red box in the top panel (Flynn et al. 1994).

To this end, the EOS Interdisciplinary Science (IDS) Global Assessment of Active Volcanism, Volcanic Hazards, and Volcanic Inputs to the Atmosphere investigation (Peter Mouginis-Mark, PI) is working in close cooperation with the MODIS science team to develop a thermal anomaly trigger to identify active volcanic eruptions and lava flows (Figure 8.11). Once a volcanic eruption is identified, ASTER will be targeted to observe these volcanoes using the high-spatial-resolution thermal-infrared radiometer.

Numerous issues remain regarding the type of radar observations that are needed to enable radar interferometry experiments to be successful in the detection and mapping of volcanic hazards. The temporal frequency of the repeat-pass, the errors due to ionospheric perturbations and atmospheric water vapor, and the surface characteristics of volcanoes are all believed to be important, but none of these issues have been rigorously investigated. We can draw on the experience with the ERS-1 and the Shuttle Imaging Radar-C (SIR-C)/X-band Synthetic Aperture Radar (X-SAR) missions to make some recommendations for the use of future radars. However, it is clear that a combination of orbital radar observations and Global Positioning System (GPS) measurements in the field are both required for geodynamics and topographic analyses for two reasons. First, as was demonstrated with the analysis of the Landers earthquake data (Zebker et al. 1994), the radar-derived deformation map provides only line-of-sight changes with poor tem-

poral resolution. GPS data from well-documented sites are needed to provide the 3-axis ground movement and to provide a continuous record of ground deformation against which the radar data can be compared. Second, the neutral atmosphere will have a significant effect on the radar interferometry because the moisture in the atmosphere can induce a time delay equivalent to ground movement up to ~30 cm, which is far in excess of the ground movement that is typically expected from a dormant volcano (except during catastrophic eruptions). New techniques have been developed that use the time-delay information contained within the GPS signal to determine the water vapor content of the atmosphere (Bevis et al. 1994, unpublished data). If such measurements were to be obtained concurrent with imaging radar data for an interferometry experiment, it would be possible to remove this uncertainty in the resultant radar deformation map. For the detection and evaluation of volcanic hazards in the air due to eruption plumes, additional work is needed to determine why some plumes can be detected using the temperature-difference method pioneered using the Advanced Very High-Resolution Radiometer (AVHRR) data. This technique will incorporate MODIS Thermal Infrared (TIR) data to more accurately determine the silicate abundance within the plume, and the height, temperature, and topography of the plume. MISR, GLAS, HIRDLS, and Along-Track Scanning Radiometer (ATSR) (on ERS-2) data will also be used to assess the height and topography of the plume.

8.3 Required measurements and data sets

8.3.1 *Stratospheric aerosols*

For climate monitoring and prediction purposes, we need to be able to measure the aerosol loading between 40 km and the tropopause (Table 8.1). Column optical depth should be measured with a horizontal spatial resolution of 400 km and an accuracy of 0.001, which is about the natural background level. Higher spatial resolution would be useful for understanding the transport characteristics of the stratospheric aerosol, but this does not appear feasible with the limb-sounding measurement techniques necessary to acquire the required accuracy. The vertical distribution should be measured with a vertical resolution of 1 km.

Because of the limited mass of the stratosphere, stratospheric aerosol optical depths are generally small but can be measured accurately with high vertical resolution with limb-sounding instruments. SAGE III obtains high accuracy and precision in aerosol extinction measurements by solar or lunar occultation through the limb of the atmosphere. The longwave emission techniques used by HIRDLS offer greater spatial coverage and more-frequent sampling, but with somewhat reduced absolute accuracy. HIRDLS also offers some advantages in the spectroscopy of aerosols and detection of aerosols with radii less than 0.1 μm . Very high vertical resolution of about 1 km is possible with these techniques. Because of

TABLE B.1

PARAMETER NAME	UNITS	ACCURACY ABS::REL	TEMPORAL RESOLUTION	HORIZONTAL RESOL::COVER	VERTICAL RESOL::COVER	COMMENTS
SAGE III Aerosol Extinction Profiles (7 wavelengths)	1/km	5% :: 5%	1 profile/ (2 min), 30/day	<2 × <1 deg :: Global	1 km :: 0-40 km	
HIRDLS Aerosol Extinction Coefficient	1/km	5-10% :: 1-10%	2 global maps /day [d, n]	400 × 400 km :: Global	1 km :: 5-60 km (given accuracies for 7-30 km)	

Stratospheric aerosols

TABLE B.2

PARAMETER NAME	UNITS	ACCURACY ABS::REL	TEMPORAL RESOLUTION	HORIZONTAL RESOL::COVER	VERTICAL RESOL::COVER	COMMENTS
MODIS Aerosol Optical Depth, Spectral	dimensionless	0.05 (Ocean) 0.1(Land) :: 0.05 (Ocean) 0.1(Land)	1/day	50 × 50 km; 5 × 5 km :: Land; Ocean	N/A :: Atmos	
MODIS Aerosol Size-distribution (Radius-Dispersion)	µm, dimensionless	30-50% :: 30-50%	1/day	5 × 5 km :: Ocean	N/A :: Atmos	
MISR Optical Depth, Aerosol, Tropospheric	dimensionless	Larger of 0.05, 10% ::	1/(2-9 day) [d]	17.6 km :: Global	Column :: Atmos	
MISR Particle Size Distribution Parameters	various	N/A ::	1/mission (possible 1/yr update)	N/A :: N/A	N/A :: N/A	SCF generated
GLAS Aerosol Vertical Structure (Profile)	/m	20% ::	1/(2-16 day)	2-100 km :: Global	150 m :: Atmos	
GLAS Thin Cloud/ Aerosol Optical Depth	dimensionless	20% ::	1/(2-16 day)	2-100 km :: Global	N/A :: Atmos	
EOSP Aerosol Optical Thickness	dimensionless	0.05 :: 10%	1/day [d]	40 km :: Global	Column :: Atmos	
EOSP Aerosol Particle Size	µm	25% :: 25%	1/day [d]	100 km :: Global	N/A :: Aerosol_ layer	Research product
EOSP Aerosol Refractive Index	dimensionless	0.03 :: 0.03	1/day [d]	100 km :: Global	N/A :: Aerosol_ layer	Research product
EOSP Aerosol Profile	dimensionless	N/A ::	1/day [d]	100 km :: Global	:: Atmos	Research product
OMI Aerosol Optical Depth at 386 nm	dimensionless	0.05 :: 0.02 (for PBL aerosols) TBD (for others)	1/day [d]	13 × 24 km :: Global	N/A :: Atmos	Research product
OMI Aerosol Index	dimensionless	N/A ::	1/day [d]	13 × 24 km :: Global	N/A :: 1 km and up	For automated detection of volcanic ash, smoke & dust

Tropospheric aerosols

TABLE B.3

PARAMETER NAME	UNITS	ACCURACY ABS::REL	TEMPORAL RESOLUTION	HORIZONTAL RESOL::COVER	VERTICAL RESOL::COVER	COMMENTS
OMI SO ₂	mol/cm ²	2E16 :: 1E16 (except PBL) 4E16 :: 2E16 (in PBL)	1/day [d]	13 × 24 km :: Global	50 mb :: 1 km and up	Automated detection
MLS SO ₂ Concentration	mixing ratio	5-10% :: 3 ppbv	2 per day day & night	400 km :: Global	1-3 km 15-40 km	

Sulfur dioxide concentration

the long pathlength through the limb, the threshold for detection is quite low.

8.3.2 Tropospheric aerosols

To provide an adequate data set for detecting trends in climate forcing caused by tropospheric aerosols we require a measurement accuracy for optical depth of 0.01 (Table 8.2). In addition to optical depth, information on aerosol size and vertical distribution would be very valuable. The primary mechanism for observing aerosols from space is through the solar radiation that they scatter back to space. This backscattered radiation is weak and is best observed under cloud-free, sunlit conditions over a relatively dark surface. For these reasons, a scanning instrument with good spatial resolution is desirable for acquiring clear scenes. Spectral, angular, and polarization properties of the backscattered sunlight can provide information on the amount and character of the aerosol. In addition, in UV the interaction between the strong molecular scattering and strongly UV-absorbing aerosols (volcanic ash, smoke, and mineral dust) can help in separating these aerosols from other aerosol types. With the visible channels on MODIS it will be possible to determine aerosol optical depth with an accuracy of 0.05 over oceans, and also to determine two parameters of the size distribution such as mean radius and radius dispersion with accuracies of 30 to 50%. With MISR, visible radiance will be observed at 4 frequencies and at 9 angles, so that both spectral and angular information can be used to determine aerosol optical depth and properties at a location. Neither of these instruments, however, will give very useful data on the vertical distribution of the aerosols. GLAS is an active laser that will provide very good information on the altitude of the aerosols, but only along a line traced on the Earth's surface by the nadir-staring instrument, since it does not scan across track. GLAS is also able to determine the optical thickness of thin clouds or aerosols. EOSP will utilize polarization information as well as spectral and angular information. It is hoped that this will allow the measurement accuracy requirement of 0.01 in optical depth to be achieved. Polarization data will also allow more information about the other physical properties of the aerosol to be estimated. Finally, the OMI instrument will help in the detection of aerosols in conditions where the other techniques become unreliable, namely over arid and semi-arid areas. In addition, it will detect highly UV absorbing aerosols over snow and underlying clouds.

8.3.3 Volcanic aerosol precursor gases

An important precursor gas to stratospheric volcanic aerosols is SO₂. The global distribution of this gas in the

stratosphere will be measured by MLS. The Ozone Measuring Instrument (OMI) will measure the column amount of SO₂ using reflected UV radiation (Table 8.3).

MLS will also map the concentration of HCl, which will help answer the question of whether HCl can be injected into the stratosphere by volcanoes. The Tropospheric Emission Spectrometer (TES) will be capable of measuring SO₂ and other aerosol precursor gases such as H₂S and COS over regional areas in the troposphere, and specific volcanoes have been planned as targets to be monitored for creation of these gases.

8.3.4 Volcanic hazards

For deformation monitoring and change detection of volcanoes, we will need repeat-pass orbital radar interferometry data from foreign partner platforms (e.g., ENVISAT's ASAR). Surface determination at the sub-centimeter scale must be studied at high spatial resolution (~25 m/pixel) over areas measuring ~30 × 30 km in size. L-band data (from the Advanced Land Observation Satellite [ALOS]) as well as C-band data (from the Canadian Synthetic Aperture Radar Satellite II [Radarsat II] and the European Space Agency's Environmental Satellite [ENVISAT]) would be preferable to single-wavelength coverage due to the ease of phase unwrapping of the longer wavelength data sets in areas of high topography, such as the landscapes frequently encountered in volcanic areas.

Ground deformation on the order of 1-6 cm/year is expected at ~50 sites around the world each measuring ~30 × 30 km in size, so that Synthetic Aperture Radar (SAR) data need to be collected with well-constrained orbit baselines (within ~50 cm for C-band and ~300 m for L-band). Due to atmospheric effects on the SAR phase data, redundancy of observations is required so that atmospheric water vapor effects can be removed. In order to achieve this, SAR data should be collected over each site about once per month for each radar system.

Radars can also be used to derive DEMs of volcanoes for use with numerical models that predict the flow paths of lahars and pyroclastic flows (see Figure 8.8). Advanced Synthetic Aperture Radar (ASAR), Radarsat II, and ALOS data will all permit elevation models to be derived of the hazardous volcanoes (~50 worldwide). These DEMs can be augmented by stereo coverage from ASTER, which will provide the higher-spatial-resolution (15 m) coverage that is more effective in areas of high relief (i.e., complementary to radar-derived DEMs, which are more accurate in low-relief areas).

Thermal anomalies associated with new lava flows will be detected by MODIS, and will be studied at higher spatial resolution by the Advanced Spaceborne Thermal Emission and Reflection Radiometer (ASTER) and the

Enhanced Thematic Mapper Plus (ETM+). The MODIS data stream will be searched continuously as part of the Level 1 data processing, providing worldwide alerts at least once per day from AM-1 and PM-1. The 1-km pixels of the TIR MODIS bands provide a good compromise between spatial resolution and data volume, since six MODIS channels have to be intercompared in order to eliminate false alarms (sun glint, snow, forest fires, etc.). Thermal IR MODIS data are required at night to resolve the area/temperature of the anomalies. Shortwave infrared (SWIR) and TIR ASTER data at 30 and 90 m, respectively, are required to map at high resolution the distribution of new flows, and to identify small thermal anomalies associated with lava domes and pyroclastic flows.

The primary health hazard associated with volcanic eruptions is the long-duration (months to years) emission of tropospheric SO₂ that produces a combination of sulfate aerosols and sulfuric acid. These aerosols can be detected with MISR bidirectional observations, as well as Advanced Along-Track Scanning Radiometer (AATSR) observations from ENVISAT. Due to the localized nature of these plumes, tropospheric aerosol maps

with a spatial resolution of 240 m are required for localized areas measuring a few hundred to 1000 km downwind.

The hazards presented by eruption clouds produced by explosive eruptions are numerous, but the most pressing concerns are the height of the plume and the dispersal pattern away from the vent. Explosive eruptions can be detected using MODIS radiance values in the thermal IR; silicate particles in the plume enable an eruption plume to be distinguished from weather clouds. MODIS visible data can provide daytime estimates of plume-top topography and, by virtue of the shadows cast by plumes (which may be 15- to 40-km high), the height of the plume can be estimated. Stereo images collected by MISR and AATSR can also provide height estimates that need to be accurate to ~200 m if air traffic is to avoid encounters with the plume. Volcanic SO₂ and ash plumes from more than 100 volcanic eruptions have been detected by TOMS since 1978 using an automated detection technique (Krueger et al. 1995; Bluth et al 1997; Seftor et al. 1997; Krotov et al. 1997). These data show that the two plumes are not always colocated and must be tracked separately. The OMI instrument will improve SO₂ detection sensi-

TABLE B.4

PARAMETER NAME	UNITS	ACCURACY Abs::REL	TEMPORAL RESOLUTION	HORIZONTAL RESOL::COVER	VERTICAL RESOL::COVER	COMMENTS
ASTER DEM	m	<50 m :: <30 m	1/eruption	15 m :: Regional	30 m :: Surface	New DEM model needed after each eruption
ASTER Thermal Anomalies	K	5 K :: 2 K	1/6 days	90 m :: Land	N/A :: Surface	Target eruptions and 50 prime sites only
ASTER Surface Radiance	% reflectance	TBD :: TBD	once, then after each eruption	15 m :: Land 30 m :: Land 90 m :: Land	N/A :: Surface	Target eruptions and 50 prime sites only
MODIS Thermal Anomalies	K	5 K :: 2 K	2/day day & night	1 km :: Land	N/A :: Surface	Continuous real-time monitoring
MISR Plume Level Reference Altitude	km	0.1 km :: 0.2 km	every available orbit during eruption	240 m :: Regional	0.1-0.2 km :: Troposphere	Collect data during eruption within plume dispersal
OMI SO ₂ Column	mol/cm ²	2E16 :: 1E16	1/day [d]	13 × 24 km :: Global	N/A :: Atmos	Automated detection
Radars Ground Deformation	cm	1 cm :: 0.3 cm	1/month	25 km :: Land	1 cm :: Land	Interferometric data from foreign SARs
Radars Surface Topography	m	10 m :: 2 m	once per eruption	25 km :: Land	2 m :: Land	Interferometric data from foreign SARs

Volcanic hazards.

tivity by an order of magnitude, allowing the detection and tracking of nearly all volcanic eruptions. It will also provide an image of ash clouds, that can be seen even in the presence of underlying weather clouds. OMI will also make a quick automated estimate of the height of these clouds to within 50 mb, which may be refined by manually examining high spatial resolution images from other instruments (MODIS, MISR, AATSR).

In summary, EOS (and foreign) data sets relevant to volcanic hazards are included in Table 8.4.

8.3.5 Importance of measurements collected by the missions of foreign partners

Of major importance to the analysis of volcanic hazards in the EOS era are the measurements to be made by foreign partner imaging radars. ERS-1, ERS-2, Radarsat, the Japanese Earth Remote-Sensing Satellite-1 (JERS-1), ENVISAT ASAR, ALOS, and Radarsat II will all provide crucial data that are unavailable from EOS due to the lack of a NASA radar. In addition to providing all-weather, day/night imaging capabilities, these foreign radars provide the opportunity to collect topographic and ground deformation information on active volcanoes.

These foreign radars provide complementary information to each other, by virtue of their different wavelengths (C-band or L-band), incidence angles (23-60°), and operating modes (spatial resolutions). Differences in the orbit altitude also mean that the frequencies of repeat orbits, which are needed in order to coherently intercompare the radar phase data, vary from 24 to 44 days. Operating in the Scanning Synthetic Aperture Radar (SCANSAR) mode, Radarsat also enables images with different spatial resolutions (25-100 m/pixel) and swath widths (100-500 km) to be obtained, thereby enabling a given target to be imaged more often than from fixed-incidence-angle radars, albeit with different geometries that preclude interferometric measurements.

Another important aspect of the foreign partner platforms is the enhancement of the temporal coverage of transient phenomena such as eruption plumes. Given

that the primary energetic phase of an explosive eruption as it injects material into the stratosphere is measured in hours, it is quite likely that neither AM-1 nor PM-1 will observe the event during its "formative stage." Given the different imagers on board ENVISAT and ALOS, visible and near-infrared data from these foreign partner spacecraft may indicate an eruption earlier than EOS. Every data source that is available should be used to reassemble the temporal history of an eruption, particularly the larger Pinatubo-style events that have regional-to-hemispheric effects on the atmosphere.

International satellite sensors enabling remote sensing of tropospheric aerosols include the Medium-Resolution Imaging Spectrometer (MERIS), Global Imager (GLI), Ocean Color and Temperature Scanner (OCTS), Polarization and Directionality of Earth's Reflectances (POLDER), and GOME (Global Ozone Monitoring Experiment). In addition to augmenting the sampling strategy of EOS sensors (MODIS, MISR, and EOSP), these sensors offer enhanced capabilities in specific areas. GLI, to be launched on ADEOS II, contains 36 spectral bands (comparable to MODIS), with more bands (6 vs. 2) at 250-m resolution, but fewer bands in the longwave region past 12 μm . MERIS is primarily an ocean color sensor, with tilt capability, and POLDER has polarization imaging capability that enables observations of the same Earth target from 12 directions during a single satellite pass. These sensors provide additional complementary information to the tropospheric aerosol properties derived from EOS sensors.

For stratospheric aerosols, in addition to HIRDLS and SAGE III, complementary information will be provided by the Improved Limb Atmospheric Spectrometer (ILAS) on ADEOS II and Sciamachy and GOMOS on ENVISAT. In most of the foreign partner instruments mentioned above, EOS investigators are actively engaged as members of the science teams of these sensor systems. This provides not only additional linkages to the algorithm development progress, but also cooperation in coordinated calibration/validation programs.

8.4 EOS contributions: Expected improvement in knowledge and national benefit

8.4.1 *Monitoring of volcanic eruptions and aerosols and their effects on climate*

Observations acquired by EOS instruments will provide continuous global monitoring of volcanic eruptions. For the first time, we will be able to monitor the entire process of injection and dispersal, and the chemical/physical evolution of volcanic materials in the atmosphere. MODIS, MISR, OMI, ASTER, ETM+, and EOS-era radar instruments will be used to characterize the number, location, style, and duration of eruptions. Large eruptions will be studied with several EOS instruments, and some will be targeted for high-resolution observations by ASTER, ETM+, and MISR. Plume top altitude and topography obtained from MODIS, HIRDLS, and MISR will allow us to test physical models of plume rise and dispersal.

During the EOS era, we will be able to make a complete inventory of the gases, ash, and other aerosols that reach the stratosphere versus the troposphere. Measurements of SO₂ column abundance will continue to be produced for large eruptions using data from TOMS. This will be supplemented by measurements using TES, MLS, OMI, and ASTER, which can detect lower abundances of SO₂ than TOMS, and which also provide vertical distribution information in the stratosphere (MLS) and troposphere (TES). MLS on EOS will have the advantage of daily coverage at high latitudes in both hemispheres, a significant improvement over MLS on UARS which only looks in one direction at a time. In addition to SO₂, a major new advance will be our ability to measure several other volcanic gas species from satellites, including H₂S (Atmospheric Infrared Sounder [AIRS], Tropospheric Emission Spectrometer [TES]), HF (TES, MLS), HCl (TES, MLS), and CO and COS (TES). Measurements of these other gas species are important for both hazard mitigation and analysis of climate effects.

Several EOS instruments will monitor stratospheric and tropospheric aerosols, each resulting in different types of aerosol data products at different spatial and vertical resolutions (SAGE III, EOSP, MISR, MODIS, OMI, GLAS, HIRDLS). Rather than having to rely so heavily on lidar measurements collected from isolated ground stations as we did for Mt. Pinatubo and El Chichón, EOS will provide us with a complete global picture of aerosol distribution and properties. Improved measurements of stratospheric aerosol abundance and spatial distribution will provide a better understanding of their role in heterogeneous chemical reactions that destroy ozone, and the impact of volcanic aerosols on high-altitude clouds.

When large eruptions occur during the EOS era, we will be able to directly determine how the chemistry, temperature, and dynamics of the atmosphere are affected. The comprehensive nature of EOS will allow us to separate volcanic signals in the climate record from those produced by El Niño-Southern Oscillation, monsoons, and human activities. The 15 years of continuous measurements by MODIS, the Clouds and the Earth's Radiant Energy System (CERES), and SAGE III will provide an important record of the effect of volcanic aerosols on the Earth's radiation budget (CERES), and on global vertical profiles of atmospheric temperature and composition (MODIS and SAGE III). Other instruments (AIRS/Advanced Microwave Sounding Unit [AMSU]/Humidity Sounder Brazil [HSB], MLS, TES, and HIRDLS) will provide more-detailed information over a 6-12-year time period concerning changes in atmospheric temperature and composition that may result from volcanic eruptions. The EOS IDS Four-Dimensional Atmospheric-Ocean-Land Data Assimilation System (Richard Rood, PI) investigation will provide an internally consistent data set of atmospheric parameters for assessing climate effects of large eruptions and will provide wind information needed to analyze the dispersal of volcanic clouds.

8.4.2 *Improved assessment of volcanic hazards on the ground and in the air*

The range of volcanic hazards that can be studied by EOS is very large. The hazards include the long-term changes in the inflation rate of the volcano (an indication of impending eruptions), the likely paths of lava flows, lahars and pyroclastic flows, the radiative flux of active lava flows, the ratio of gases from primary melts (indicators of new magma reaching the near-surface), and the possibility of aircraft encountering an eruption.

In qualitative terms, EOS will provide the most complete near-real-time inventory of global eruptions thus far. Many (~30-50%) lava-producing eruptions may currently go unreported, and some may have great impact on local populations. MODIS data will enable this eruption inventory to be timely (same day) and near global in coverage.

Topographic mapping and deformation studies will rely to a considerable degree on foreign radars (e.g., ENVISAT ASAR). Only via radar interferometry can centimeter-scale deformation be detected from orbit. This deformation may be detected several weeks to months in advance of an eruption, enabling local authorities to be warned and, if required, evacuation plans to be developed.

Digital elevation models derived from stereo ASTER data will also aid in the prediction of lava flow and lahar flow paths.

MODIS, MISR, and OMI data will enable large eruption plumes to be studied in unprecedented detail compared to existing AVHRR analyses. Since each eruption is unique in terms of magma chemistry, vent geometry, volume erupted, and atmospheric conditions, a direct comparison between EOS investigations and earlier studies is not possible. However, improvements in spectral resolution of MODIS compared to AVHRR will enable more-subtle variations of silicate materials in the plume to be studied, thereby providing warning to nearby aircraft that the plume is dangerous if ingested by the engines. MISR data will also enable, via parallax measurements, the plume height to be determined to within a few hundred meters, thereby better defining the hazardous region that aircraft should avoid (see Figure 8.10).

Health hazards are a poorly studied aspect of the effects of volcanoes. Long-duration (months to years) eruptions can increase respiratory problems by more than an order of magnitude, and affect tens of thousands of people. MISR and EOSP data will be particularly good at detecting such low-level plumes via multi-zenith-angle studies of the scattering properties of the atmosphere.

8.4.3 Improved knowledge of the global frequency and magnitude of volcanic eruptions

Global coverage provided by MODIS will give the first comprehensive worldwide inventory of volcanic eruptions. Use of near-real-time processing of a segment of the MODIS data stream will enable the inventory to be made available to the world's volcanologists in only a few hours after data acquisition, thereby enabling field observations of certain eruptions that were previously unreported from the ground.

Major advances in the knowledge of the thermal properties of lava flows, volcanic domes, lava lakes, and summit water lakes will also be derived. In this instance, ASTER will provide the most important data set, due to the greater spatial resolution. However, the high dynamic range of the mid-IR (3.9 μm) MODIS data will permit the solution of both temperature and area for many hot volcanic targets. In many cases, the total energy released from an eruption has to be estimated from post-eruption assessments of the volume of material erupted (Figure 8.11). MODIS, ETM+, and ASTER will facilitate quantitative measurements of radiative flux from lava flows, enabling the magnitude of different eruptions to be intercompared.

Explosive eruptions will also be quantified by EOS for the first time. The height of eruption plumes will be

measured by MISR, MODIS, and GLAS, and the amount of SO_2 erupted will be measured by TOMS and OMI. TOMS data provide the longest continuous record (1978-1994) of stratospheric SO_2 emissions from volcanoes. These data are crucial for assessing the impact of volcanoes on the stratosphere. Additional observations by Earth Probe (EP) TOMS, Meteor-3 TOMS, and OMI on EOS Chemistry-1 will extend this time series. More detailed observations of gas chemistry from an explosive eruption will also be obtained from MLS and TES.

8.4.4 Global measurements of tropospheric aerosols

The early development of EOS has been contemporaneous with a growing realization of the importance of acquiring the capability to adequately monitor the characteristics of tropospheric aerosols globally. In the past, the difficulty of satellite remote sensing of tropospheric aerosols, along with the perception that improvement in characterizing cloud radiative forcing had a much higher priority, has resulted in only a very limited effort to monitor aerosols. Indeed, the only operational aerosol data product at present is the total column optical thickness retrieved using the AVHRR instrument on the NOAA polar-orbiting environmental satellites (cf. Rao et al. 1988). That retrieval employs the traditional approach of relying on the enhanced reflectance of scattered sunlight relative to a low albedo surface (viz., the cloud-free ocean away from sun glint). The present NOAA aerosol retrieval uses only AVHRR channel-1 (0.58-0.68 μm) radiances because of the variable effects of water vapor on channel-2 (0.725-1.10 μm) radiances (cf. Rao et al. 1989; Durkee et al. 1991). With information restricted to radiance at just one wavelength, the retrieval algorithm must employ a single, standard model for the aerosol and is thus subject to potentially substantial uncertainties associated with the wide range of aerosol types and properties.

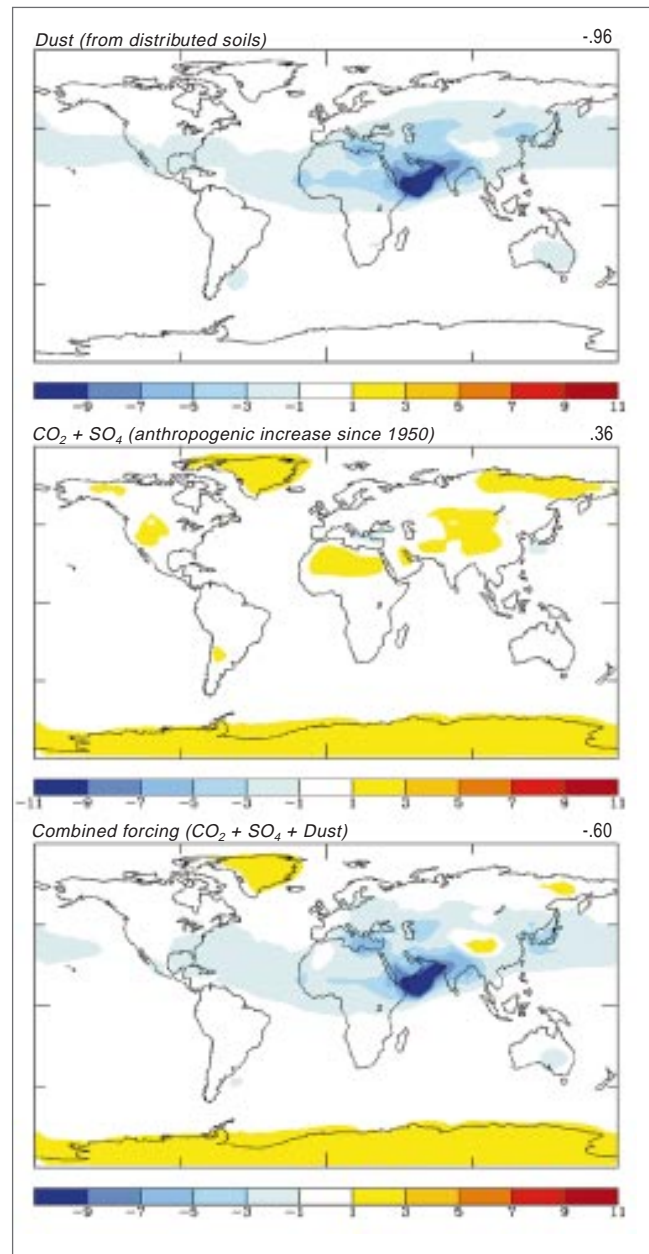
As discussed in previous sections, tropospheric aerosols must be monitored on a global basis and not just over the oceans where retrieval is somewhat easier. Furthermore, we require aerosol properties beyond just column optical thickness in order to adequately characterize their direct radiative forcing, their effect on clouds and the hydrological cycle, their sources and sinks, and their participation in atmospheric chemical processes. Because of the variability of aerosol loading for specific aerosol types and the difficult problem of distinguishing the contribution of the surface to the satellite observations, a credible program for global monitoring of tropospheric aerosols must necessarily emphasize taking advantage of as much of the information content of the scattered and reflected sunlight as possible, namely, multi-spectral and multi-angle radiance and polarization

measurements. In this regard, the EOS program offers significant advances because of its measurement capabilities that are attributable in part to serious consideration of aerosol objectives in both instrument conceptual designs and payload selection processes.

The three EOS instruments fundamental to tropospheric aerosols measurement objectives are MODIS, MISR, and EOSP. MODIS, to be flown on both the EOS AM-1 and PM-1 platforms, is a scanning spectroradiometer operating much like AVHRR but with significantly greater multi-spectral coverage, higher spatial resolution, and greatly enhanced on-board calibration capability. With 36 spectral bands covering the visible, near-infrared, and SWIR, MODIS measurements will provide aerosol optical-thickness retrievals for a broad range of wavelengths, from which we can infer information on aerosol size distribution. While aerosol retrievals with MODIS will be most straightforward and detailed over the ocean, there is the expectation that meaningful results over land can be realized by taking advantage of information on surface properties inherent in some of the spectral bands, particularly in the SWIR, and by using aerosol “climatology” or ancillary measurements to constrain aerosol models used in the retrieval algorithm. In addition, combination of MODIS with TOMS and OMI has the potential of improving MODIS retrievals over land, as well as extending the wavelength range to 340 nm for better detection of submicron particles. MODIS thermal and SWIR bands will also be useful in cloud screening (i.e., avoiding attempted aerosol retrievals for pixels that are “contaminated” with a very small cloud fraction or thin cirrus clouds).

A significant additional source of information is available from the multi-angle coverage in the plane containing the spacecraft ground track obtained from the nine cameras of the MISR instrument, which uses charge-coupled device (CCD) arrays to acquire cross-track spatial coverage in four spectral bands in the visible. MISR will be flown on the EOS AM platform series. Without resorting to any assumptions about spatial homogeneity of aerosol characteristics, the MISR views of the same location at nine zenith angles during the short time period of the spacecraft overflight can provide direct information on the aerosol angular scattering, or phase function, which is diagnostic of aerosol size dis-

FIGURE 8.12

Surface forcing (Wm^{-2}) (Tegen et al. 1996).

tribution and particle shape. Over relatively brighter, heterogeneous land surfaces, the MISR retrieval algorithm will employ an innovative technique (Martonchik and Diner 1992) based upon analysis of the spatial frequency power spectrum of the radiances over a scene with the assumption that the aerosol typically will produce no contribution to the power at any frequencies other than the very lowest. This technique offers the prospect of satel-

lite aerosol retrievals for the most difficult of scenes, but its narrower swath width requires 16 days to achieve full global coverage.

On the second of the EOS AM platforms, advanced versions of MODIS and MISR will be joined by EOSP, which measures the linear polarization as well as the radiance at 12 spectral bands in the visible, near-infrared, and SWIR. The advantage of polarimetry is both the very high measurement accuracy possible because linear polarization is a ratio of orthogonal intensities, and the fact that polarization is very sensitive to particle microphysics (Hansen and Travis 1974). Previous experience with polarimetry on planetary missions has demonstrated aerosol-retrieval capabilities in situations where radiance-only measurements are subject to model uniqueness problems. For example, the analysis of Cloud Photopolarimeter measurements from the Pioneer Venus Orbiter permitted the retrieval of small-particle (0.25 μm radius) haze of optical thickness on the order of 0.02 extending above the main cloud of 1- μm particles with concurrent retrieval of refractive indices. Although retrievals of terrestrial tropospheric aerosols over land must deal with potentially variable and uncertain contributions from the surface reflectivity and polarization signatures, evidence that the polarized component of sunlight scattered from vegetation comes almost entirely from light that is specularly reflected at the leaf surfaces (Vanderbilt et al. 1985), together with the broad EOSP spectral coverage, suggests that the surface contributions can be appropriately treated.

Perhaps as important as the significant advance in EOS instrument capabilities with respect to tropospheric aerosol measurements, is the underlying EOS philosophy that emphasizes instrument calibration and retrieved product validation. Because of the inherent difficulties of satellite aerosol retrievals even with greatly improved capabilities, it is recognized that appropriate validation should include comparison of coincident measurements with ground-based sunphotometer and/or shadow-band radiometers. Remote sensing of aerosol properties with such upward-looking instruments has been demonstrated to be a very reliable technique and will be key to establishing the quality of the satellite-derived aerosol products (Kaufman et al. 1994). Moreover, the envisioned networks of ground-based instruments (e.g., Aerosol Robotic Network [AERONET]; Holben et al. 1996) will provide important information on diurnal variations of the concentration and properties of aerosols at the selected sites. It is also expected that the EOS validations will include a number of coordinated campaigns that employ in situ sampling of aerosols, both at the ground and from aircraft, to be compared with the satellite and ground-based instru-

ment remote sensing of aerosol characteristics. EOS support of such activities as a major part of the validation objectives is fundamental to the realization of appropriate global monitoring of tropospheric aerosols.

8.4.5 Assessment of the role of tropospheric aerosols in climate change

One of the greatest uncertainties in climate forcing is that due to tropospheric aerosols (e.g., Charlson et al. 1992; Charlson and Wigley 1994; IPCC 1995). Aerosols cause a direct climate forcing by reflecting sunlight to space and absorbing solar and terrestrial radiation in the atmospheric column, and an indirect climate forcing by altering cloud properties. Existence of the latter effect is supported by satellite observations of increased cloud brightness in ship wakes (Coakley et al. 1987), satellite observations of land-ocean and hemispheric contrasts of cloud droplet sizes (Han et al. 1994, 1996), and in situ data concerning the influence of aerosol condensation nuclei on clouds (Radke et al. 1989; King et al. 1993, 1995). Sulfate aerosols originating in fossil-fuel burning may produce a global climate forcing of the order -1 Wm^{-2} (Charlson et al. 1991; Houghton et al. 1996), and aerosols from biomass burning could conceivably produce a comparable forcing (Penner et al. 1992). Wind-blown dust, influenced by anthropogenic activities, has long been suspected of being an important forcing on some regional climates (Tanré et al. 1984; Joseph 1984; Coakley and Cess 1985; Tegen and Fung 1994). Tegen et al. (1996) estimate surface forcing caused by dust from disturbed soils is currently on the order of -1 Wm^{-2} , which is comparable in magnitude to the current effect of CO_2 and sulfate aerosols (Figure 8.12). It has also been suggested (Jensen and Toon 1992; Sassen 1992) that volcanic aerosols sedimenting into the upper troposphere may alter cirrus cloud microphysics, thus producing a possibly significant climate forcing, which could either be positive or negative. Unfortunately, no global data exist that are adequate to define quantitatively any of these aerosol climate forcings.

Aerosols can be seen against the dark ocean surface by the imaging instruments on present operational meteorological satellites (Rao et al. 1988; Jankowiak and Tanré 1992). For example, these images clearly show Sahara/Sahelian dust spreading westward from Africa, summertime sulfate aerosols moving eastward from the United States, and aerosols from seasonal biomass burning in the tropics. Similar data over both land and oceans can be seen in the TOMS images (Herman et al. 1998). However, the nature and accuracy of these data are inadequate to define the climate forcing, and, indeed, the

observed optical thicknesses may be in part due to thin cirrus clouds. The climate forcing issue requires aerosol data of much higher precision, including information on aerosol altitude and aerosol physical properties such as size and refractive index. Cloud properties, including optical thickness, particle size, and phase, must be monitored simultaneously to very high precision, so that the temporal and spatial variations of aerosols and clouds can be used to help define the indirect aerosol climate forcing.

MISR and MODIS on the EOS AM-1 spacecraft will provide aerosol optical-thickness measurements substantially better than aerosol information available from current instruments. Furthermore, MODIS will provide substantial improvements on current abilities to derive cloud optical and microphysical properties (see Chapter 3). The estimated accuracy of optical-thickness retrievals, 0.03 to 0.05, will contribute to aerosol process studies in regions of moderate to heavy aerosol loading. The higher accuracies needed for determination of aerosol climate forcing, about 0.01 (Hansen et al. 1995), and microphysical aerosol properties (refractive index, particle shape, and particle size) will be provided by EOSP, scheduled for the EOS AM-2 spacecraft. EOSP has also been proposed for flight on a microsat (Hansen et al. 1995) along with a Michelson interferometer that would be capable of measuring small changes in cloud optical and microphysical properties. A satellite-borne lidar would be an ideal complement to these latter instruments, providing a precise determination of vertical layering of aerosols and clouds. To this end, GLAS on the ICESat-1 spacecraft will provide valuable information on the vertical and spatial extent of significant stratospheric and tropospheric aerosol layers.

8.4.6 Inclusion of aerosol effects in model predictions of global climate change

Aerosol effects can be included in global climate model calculations, provided the aerosol amount, distribution, and optical properties are known. This knowledge is only available after the fact in the case of volcanic eruptions, but study of de facto volcanic aerosol injections can be valuable as a check on our understanding of the climate response to a radiative forcing. Calculations with simplified climate models have suggested that the largest volcanoes of the past century could have caused a global cooling of up to 0.5°C (Schneider and Mass 1975; Hunt 1977; Hansen et al. 1978; Robock 1983; MacCracken and Luther 1984). The mean observed global temperature response after the five largest eruptions is a cooling of about 0.25°C (Hansen et al. 1995), but the aerosol data and observed temperatures are not sufficiently precise to allow

determination of whether a significant discrepancy exists between the models and the observed climate change.

The 1991 eruption of Mt. Pinatubo provides the best chance to date for testing climate models against observed volcanoes. Climate simulations carried out immediately after the eruption with a GCM (Hansen et al. 1992) predicted a global cooling of about 0.5°C. Observations found a cooling of about 0.5°C over land and globally in the lower troposphere, but a smaller surface response over the ocean yielded a global surface cooling of only about 0.3°C (Hansen et al. 1995). At least part of the difference between model and observations can be accounted for by inaccuracy of the aerosol size distribution assumed in the Hansen et al. (1992) calculations, which yielded a maximum forcing just over 4 Wm⁻². More-precise aerosol data (Lambert et al. 1993; McCormick et al. 1995) now available yield a global forcing of about 3.5 Wm⁻² (Hansen et al. 1995); this smaller forcing is also more consistent with ERBE measurements of global radiative flux anomalies at the top of the atmosphere (Minnis et al. 1993). Comprehensive analyses of the Pinatubo case with the most realistic atmosphere-ocean models have yet to be made.

Modeling of tropospheric aerosols presents a greater challenge because of the large number of heterogeneously-distributed aerosols and the evidence that aerosols can alter cloud properties. The predominant anthropogenic aerosol is probably sulfate originating from the burning of fossil fuels. The regional distribution of these aerosols can be estimated from aerosol-formation models (Langner and Rodhe 1991) and used to calculate an approximate anthropogenic sulfate climate forcing (Kiehl and Briegleb 1993). There is a qualitative consistency among the regions of heavy aerosol amounts (eastern United States, Europe, and China), calculated aerosol coolings (Taylor and Penner 1994), and the observed temperature change of the past century (Karl et al. 1995).

The difficult task of realistically including aerosol effects in projections of future climate change requires quantitative knowledge of all the significant changing aerosols, including aerosols from biomass burning, dust from arid regions, biogenic aerosols, and industrial soot. Moreover, it is necessary to understand the aerosol effects on cloud properties. The challenge for EOS is to provide the data necessary to allow understanding and prediction of aerosol changes, as an essential aspect of assessing the causes of climate variability and climate change.

8.4.7 Advertent climate modification by aerosols

The human response to global change can take one of three generic forms: modify the human actions that are causing global change in order to mitigate the magnitude of the future changes, adapt to the changes that are caused, or introduce a new human action that will compensate for the causative action. The last option may be called the geo-engineering approach. For reducing the effect of greenhouse gases on climate warming, two approaches have been suggested (Committee on Science, Engineering, and Public Policy [COSEPUP] 1992): introducing aerosols into the stratosphere to act as a direct reflector of solar radiation, and introducing aerosols into the troposphere to increase the reflectivity of clouds. These two actions have the advantage of being reversible, since once the introduction of aerosol ceases, the aerosol burden will return to natural levels within a few weeks in the troposphere and within a year or so in the stratosphere. The Earth system is too poorly understood at present to enable all the consequences of such approaches to be predicted. However, EOS studies of aerosols and clouds will help improve understanding of the climate system to the point where the consequences of these actions to contravene the greenhouse warming may be predicted with reasonable confidence. In addition, EOS instruments will provide the technology necessary to monitor the levels of any such introduced aerosols and their effects on the climate system.

References

- Albrecht, B. A., 1989: Aerosols, cloud microphysics, and fractional cloudiness. *Science*, **245**, 1227–1230.
- Andreae, M. O., 1995: Climate effects of changing atmospheric aerosol levels. *World Survey of Climatology XVI: Future Climates of the World*, A. Henderson-Sellers, Ed., Elsevier.
- Andreae, M. O., E. V. Browell, M. Garstang, G. L. Gregory, R. C. Harris, G. F. Hill, D. J. Jacob, M. C. Pereira, G. W. Sachse, A. W. Setzer, P. L. Silva Dias, R. W. Tablot, A. L. Torres, and S. C. Wofsy, 1988: Biomass burning emissions and associated haze layers over Amazonia. *J. Geophys. Res.*, **93**, 1509–1527.
- Andreae, M. O., B. E. Anderson, D. R. Blake, J. D. Bradshaw, J. E. Collins, G. L. Gregory, G. W. Sachse, and M. C. Shipman, 1994: Influence of plumes from biomass burning on atmospheric chemistry over the equatorial and tropical South Atlantic during CITE 3. *J. Geophys. Res.*, **99**, 12,793–12,808.
- Artaxo, P., F. Gerab, M. A. Yamasoe, and J. V. Martins, 1994: Fine mode aerosol composition at three long-term atmospheric monitoring sites in the Amazon Basin. *J. Geophys. Res.*, **99**, 22,857–22,868.
- Asano, S., 1993: Estimation of the size distribution of Pinatubo volcanic dust from Bishop's ring simulations. *Geophys. Res. Lett.*, **20**, 447–450.
- Asano, S., A. Vchiyama, and M. Shiobara, 1993: Spectral optical thickness and size distribution of the Pinatubo volcanic aerosols as estimated by ground-based sunphotometry. *J. Meteor. Soc. Japan*, **71**, 165–173.
- Benkovitz, C. M., R. C. Easter, S. Nemesure, R. Wagener, and S. E. Schwartz, 1994: Sulfate over the North Atlantic and adjacent continental regions: Evaluation of October and November 1986 using a three-dimensional model driven by observation-derived meteorology. *J. Geophys. Res.*, **99**, 20,725–20,756.
- Bevis, M., S. Businger, S. Chiswell, T. A. Herring, R. A. Anthes, C. Rocken, and R. H. Ware, 1994: GPS meteorology: mapping zenith wet delays onto precipitable water. *J. Appl. Meteor.*, **33**, 379–386.
- Blanchard, D. C., and L. D. Syzdek, 1972: Concentration of bacteria in jet drops from bursting bubbles. *J. Geophys. Res.*, **77**, 5087–5099.
- Bluth, G. J. S., W. I. Rose, I. E. Sprod, and A. J. Krueger, 1997: Stratospheric loading from explosive volcanic eruptions. *J. Geophys. Res.*, **105**, 671–683.
- Braham, R. R., Jr., 1974: Cloud physics of urban weather modification—a preliminary report. *Bull. Amer. Meteor. Soc.*, **55**, 100–106.
- Brantley, S. R., 1990: The Eruption of Redoubt Volcano, Alaska, December 14, 1989–August 31, 1990. *U. S. Geological Survey Circular*, **1061**, 33 pp.
- Browell, E. V., E. F. Danielsen, S. Ismail, G. L. Gregory, and S. M. Beck, 1987: Tropopause fold structure determined from airborne lidar and in situ measurements. *J. Geophys. Res.*, **92**, 2112–2120.
- Cachier, H., M. P. Bremond, and P. Buat-Menard, 1989: Carbonaceous aerosol from different tropical biomass burning sources. *Nature*, **340**, 371–373.
- Casadevall, T. J., 1994: Volcanic ash and aviation safety. Proc. 1st Int. Symp. on Volcanic Ash and Aviation Safety, *U. S. Geological Survey Bull.*, **2047**, 450 pp.
- Charlson, R. J., and T. M. L. Wigley, 1994: Sulfate aerosol and climatic change. *Sci. Amer.*, **270**, 48–57.
- Charlson, R. J., J. Langner, H. Rodhe, C. B. Leovy, and S. G. Warren, 1991: Perturbation of the Northern Hemisphere radiative balance by backscattering from anthropogenic sulfate aerosols. *Tellus*, **43**(AB), 152–163.
- Charlson, R. J., S. E. Schwartz, J. M. Hales, R. D. Cess, J. A. Coakley, Jr., J. E. Hansen, and D. J. Hofmann, 1992: Climate forcing by anthropogenic aerosols. *Science*, **255**, 423–430.
- Coakley, J. A., and G. Grams, 1976: Relative influence of visible and infrared optical properties of a stratospheric aerosol layer on the global climate. *J. Appl. Meteor.*, **15**, 679–691.
- Coakley, J. A., and R. D. Cess, 1985: Response of the NCAR community climate model to the radiative forcing of naturally occurring tropospheric aerosol. *J. Atmos. Sci.*, **42**, 1677–1692.
- Coakley, J. A., Jr., R. L. Bernstein, and P. A. Durkee, 1987: Effect of ship-stack effluents on cloud reflectivity. *Science*, **237**, 1020–1022.
- COSEPUP, 1992: Policy implications of greenhouse warming, mitigation, adaptation, and the science base. Panel on Policy Implications of Greenhouse Warming, Committee on Science, Engineering, and Public Policy, National Academy of Sciences, National Academy Press, 918 pp.
- Crutzen, P. J., and M. O. Andreae, 1990: Biomass burning in the tropics: Impact on atmospheric chemistry and biogeochemical cycles. *Science*, **250**, 1669–1678.
- Crutzen, P. J., L. E. Heidt, J. P. Krasnec, W. H. Pollock, and W. Seiler, 1979: Biomass burning as a source of atmospheric gases. *Nature*, **282**, 253–256.
- Deshler, T., D. J. Hofmann, B. J. Johnson, and W. R. Rozier, 1992a: Balloonborne measurements of the Pinatubo aerosol size distribution and volatility at Laramie, Wyoming during the summer of 1991. *Geophys. Res. Lett.*, **19**, 199–202.
- Deshler, T., A. Adriani, G. P. Gobbi, D. J. Hofmann, G. Di-Donfrancesco, and B. J. Johnson, 1992b: Volcanic aerosol and ozone depletion within the Antarctic polar vortex during the austral spring of 1991. *Geophys. Res. Lett.*, **19**, 1819–1822.
- Deshler, T., B. J. Johnson, and W. R. Rozier, 1993: Balloon measurements of Pinatubo aerosol during 1991 and 1992 at 41°N: vertical profiles, size distribution, and volatility. *Geophys. Res. Lett.*, **20**, 1435–1438.
- Diner, D. J., C. J. Bruegge, J. V. Martonchik, T. P. Ackerman, R. Davies, S. A. W. Gerstl, H. R. Gordon, P. J. Sellers, J. Clark, J. A. Daniels, E. D. Danielson, V. G. Duval, K. P. Klaasen, G. W. Lilienthal, D. I. Nakamoto, R. J. Pagano, and T. H. Reilly, 1988: MISR: A Multiangle Imaging Spectro-Radiometer for Geophysical and Climatological Research from EOS. *IEEE Trans. Geosci. and Remote Sens.*, **27**, 200–214.
- Diner, D. J., C. J. Bruegge, J. V. Martonchik, G. W. Bothwell, E. D. Danielson, E. L. Floyd, V. G. Ford, L. E. Hovland, K. L. Jones, and M. L. White, 1991: A Multi-angle Imaging SpectroRadiometer for terrestrial remote sensing from the Earth Observing System. *Int. J. Imaging Systems and Technol.*, **3**, 92–107.
- Durkee, P. A., D. R. Jensen, E. E. Hindman, and T. H. Vonder Haar, 1986: The relationship between marine aerosol particles and satellite-detected radiance. *J. Geophys. Res.*, **91**, 4063–4072.
- Durkee, P. A., F. Pfeil, E. Frost, and R. Shema, 1991: Global analysis of aerosol particle characteristics. *Atmos. Environ.*, **25A**, 2457–2471.
- Dutton, E. G., and J. R. Christy, 1992: Solar radiation forcing at selected locations and evidence for global lower tropospheric cooling following the eruptions of El Chichón and Pinatubo. *Geophys. Res. Lett.*, **19**, 2313–2316.
- Dutton, E. G., P. Reddy, S. Ryan, and J. J. DeLuisi, 1994: Features and effects of aerosol optical depth observed at Mauna Loa, Hawaii: 1982–1992. *J. Geophys. Res.*, **99**, 8295–8306.

- Eck, T.F., P.K. Bhartia, P.H. Hwang, and L.L. Stowe, 1987: Reflectivity of the earth's surface and clouds in ultraviolet from satellite observations. *J. Geophys. Res.*, **92**, 4287-4296.
- Eluszkiewicz, J., D. Crisp, R. Zurek, L. Elson, E. Fishbein, L. Froidevaux, J. Waters, R. G. Grainger, A. Lambert, R. Harwood, and G. Peckham, 1996: Residual circulation in the stratosphere and lower mesosphere as diagnosed from Microwave Limb Sounder data. *J. Atmos. Sci.*, **53**, 217-240.
- Evans, D. L., T. G. Farr, H. A. Zebker, J. van Zyl, and P. J. Mouginis-Mark, 1992: Radar interferometric studies of the Earth's topography. *Eos Trans. AGU*, **73**, 553, 557-558.
- Faivre-Perret, R., and F. Le Guern, 1983: Health risks linked with inhalation of volcanic gases and aerosols. *Forecasting Volcanic Events*. H. Tazieff and J. C. Sabroux, Ed., Elsevier, NY, 69-81.
- Feigl, K. L., A. Sargent, and D. Jacq, 1994: Estimation of an earthquake focal mechanism from a satellite radar interferogram: application to the December 4, 1992 Landers aftershock. *Geophys. Res. Lett.*, **22**, 1037-1040.
- Flynn, L. P., P. J. Mouginis-Mark, and K. A. Horton, 1994: Distribution of thermal areas on an active lava flow field: Landsat observations of Kilauea, Hawaii, July 1991. *Bull. Volcanology*, **56**, 284-296.
- Garrett, T. J., and P. V. Hobbs, 1995: Long-range transport of continental aerosols over the Atlantic Ocean and their effects on cloud structure. *J. Atmos. Sci.*, **52**, 1977-1984.
- Graf, H. F., I. Kirchner, A. Robock, and I. Schult, 1993: Pinatubo eruption winter climate effects: model versus observations. *Clim. Dyn.*, **9**, 81-93.
- Grainger, R. G., A. Lambert, F. W. Taylor, J. J. Remedios, C. D. Rodgers, M. Corney, and B. J. Kerridge, 1993: Infrared absorption by volcanic stratospheric aerosols observed by ISAMS. *Geophys. Res. Lett.*, **20**, 1283-1286.
- Grainger, R. G., A. Lambert, C. D. Rodgers, F. W. Taylor, and T. Deshler, 1995: Stratospheric aerosol effective radius, surface area, and volume estimated from infrared measurements. *J. Geophys. Res.*, **100**, 16,507-16,519.
- Grant, W. B., E. V. Browell, C. S. Long, L. L. Stowe, R. G. Grainger, and A. Lambert, 1996: Use of aerosols resulting from volcanic eruptions to study the tropical stratospheric reservoir, its boundary, and transport to northern latitudes. *J. Geophys. Res.*, **101**, 3,973-3,988.
- Halpert, M. S., C. F. Ropelewski, T. R. Karl, J. K. Angell, L. L. Stowe, R. R. Heim, Jr., A. J. Miller, and D. R. Rodenhuis, 1993: 1992 brings return to moderate global temperatures. *EOS Trans. AGU*, **74**, 433-439.
- Hamill, P., O. B. Toon, and C. S. Kiang, 1977: Microphysical processes affecting stratospheric aerosol particles. *J. Atmos. Sci.*, **34**, 1104-1119.
- Han, Q. Y., W. B. Rossow, and A. A. Lacis, 1994: Near-global survey of effective cloud droplet radii in liquid water clouds using ISCCP data. *J. Climate*, **7**, 465-497.
- Han, Q. Y., W. B. Rossow, J. Chou, and R. M. Welch, 1996: Indirect effect of aerosols on climate change. Submitted, *J. Geophys. Res.*
- Hansen, J. E., and L. D. Travis, 1974: Light scattering in planetary atmospheres. *Space Science Rev.*, **16**, 527-610.
- Hansen, J. E., W. C. Wang, and A. A. Lacis, 1978: Mount Agung eruption provides test of a global climate perturbation. *Science*, **199**, 1065-1068.
- Hansen, J., A. Lacis, R. Ruedy, and M. Sato, 1992: Potential climate impact of Mount Pinatubo eruption. *Geophys. Res. Lett.*, **19**, 215-218.
- Hansen, J., and 29 co-authors, 1995: A Pinatubo climate modeling investigation. NATO Advanced Science Institutes Series, Springer-Verlag.
- Hansen, J., W. Rossow, B. Carlson, A. Lacis, L. Travis, A. Del Genio, I. Fung, B. Cairns, M. Mishchenko, and M. Sato, 1995: Low-cost long-term monitoring of global climate forcings and feedbacks. *Clim. Change* (in press).
- Hao, W. M., M. H. Liu, and P. Crutzen, 1990: Estimates of annual and regional releases of CO₂ and other trace gases to the atmosphere from fires in the tropics, based on the FAO statistics for the period 1975-1980. *Fire in the Tropical Biota*, J. G. Goldammer, Ed., Springer-Verlag, Berlin, 440-462.
- Harshvardhan, and R. D. Cess, 1976: Stratospheric aerosols: effect upon atmospheric temperature and global climate. *Tellus*, **28**, 1-10.
- Hegg, D.A., P.V. Hobbs, R.J. Ferek, and A.P. Waggner, 1995: Measurements relevant to radiation forcing by aerosols on the east coast of the United States. *J. Appl. Meteor.*, **34**, 2306-2315.
- Hegg, D. A., R. J. Ferek, and P. V. Hobbs, 1993: Aerosol size distribution in the cloudy atmospheric boundary layer of the north Atlantic Ocean. *J. Geophys. Res.*, **98**, 8841-8846.
- Herman, J.R., and E. Celarier, 1997: Earth's surface reflectivity climatology at 340-380 nm from TOMS data. *J. Geophys. Res.*, **102**, 28,003-28,012.
- Herman, J.R., P. K. Bhartia, O. Torres, C. Hsu, C. Seftor, and E. Celarier, 1997: Global distribution of UV-absorbing aerosols from the Nimbus 7/TOMS data. *J. Geophys. Res.*, **102**, 16,911-16,922.
- Hobbs, P. V., 1993: Aerosol-cloud interactions. In *Aerosol-Cloud-Climate Interactions*, (P.V. Hobbs, Ed.), Academic Press.
- Hobbs, P. V., L. F. Radke, M. W. Elgroth, and D. A. Hegg, 1981: Airborne studies of the emissions from the volcanic eruptions of Mount St. Helens. *Science*, **211**, 816-818.
- Holben, B. N., E. Vermote, Y. J. Kaufman, D. Tanré, and V. Kalb, 1992: Aerosols retrieval over land from AVHRR data—Application for atmospheric correction. *IEEE Trans. Geosci. Remote Sens.*, **30**, 212-222.
- Holben, B. N., T. F. Eck, I. Slutsker, A. Setzer, A. Pereira, E. Vermote, J. A. Reagan, Y. J. Kaufman, and D. Tanré, 1995: Sunphotometer network measurement of aerosol properties in the Brazilian Amazon. Submitted to *Remote Sens. Environ.*
- Holben, B. N., T. F. Eck, I. Slutsker, D. Tanré, J. P. Buis, A. Setzer, E. Vermote, J. A. Reagan, Y. J. Kaufman, T. Nakajima, F. Lavenue, and I. Jankowiak, 1996: Automatic sun and sky radiometer system for network aerosol monitoring. *Remote Sens. Environ.*, in press.
- Holasek, R. E., and W. I. Rose, 1991: Anatomy of 1986 Augustine volcano eruptions as recorded by digital AVHRR weather satellite data. *Bull. Volcanology*, **53**, 420-435.
- Hoppel, W. A., J. W. Fitzgerald, G. M. Ferick, and R. E. Larson, 1990: Aerosol size distribution and optical properties found in the marine boundary layer over the Atlantic Ocean. *J. Geophys. Res.*, **95**, 3659-3686.
- Houghton, J. T., L. G. Meira Filho, B. A. Callander, N. Harris, A. Kattenberg, and K. Maskell, 1996: Climate Change 1995: The Science of Climate Change, 572, Intergovernmental Panel on Climate Change, Cambridge.
- Hunt, B. G., 1977: A simulation of the possible consequences of a volcanic eruption on the general circulation of the atmosphere. *Mon. Wea. Rev.*, **105**, 247-260.
- IPCC, 1995: Climate Change 1994: *Radiative Forcing of Climate Change and an Evaluation of the IPCC 92 Emission Scenarios*, J. T. Houghton, L. G. Miera Filho, J. Bruce, H. Lee, B. A. Callander, E. Haites, N. Harris, and K. Maskell, Eds., Intergovernmental Panel on Climate Change, Cambridge University Press, 339 pp.
- Jaenicke, R., 1993: Tropospheric aerosols. In *Aerosol-Cloud-Climate Interactions*, (P. V. Hobbs, Ed.), Academic Press.

- Jankowiak, I., and D. Tanré, 1992: Satellite climatology of Saharan dust outbreaks: Method and preliminary results. *J. Climate*, **5**, 646–656.
- Jensen, J. E., and O. B. Toon, 1992: The potential effects of volcanic aerosols on cirrus cloud microphysics. *Geophys. Res. Lett.*, **19**, 1759–1762.
- Joseph, J. H., 1984: The sensitivity of a numerical model of the global atmosphere to the presence of desert aerosol. *Aerosols and their Climatic Effects*. H. E. Gerber and A. Deepak, Eds., Deepak Publ., 215–226.
- Karl, T. R., R. W. Knight, G. Kukla, and J. Gavin, 1995: Evidence for radiative effects of anthropogenic sulfate aerosols in the observed climate record. *Aerosol Forcing of Climate*. R. J. Charlson and J. Heintzenberg, Eds., John Wiley & Sons, 363–382.
- Kaufman, Y. J., 1978: Influence of the atmosphere on the contrast of Landsat images. *Space Res.*, XVIII, Oxford, 65–69.
- Kaufman, Y. J., and T. Nakajima, 1993: Effect of Amazon smoke on cloud microphysics and albedo. *J. Appl. Meteor.*, **32**, 729–744.
- Kaufman, Y. J., and D. Tanré, 1994: Effect of variations in supersaturation on the formation of cloud condensation nuclei. *Nature*, **369**, 45–48.
- Kaufman, Y. J., and B. N. Holben, 1995: Hemispherical backscattering by biomass burning and sulfate particles derived from sky measurements. Submitted to *J. Geophys. Res.*
- Kaufman, Y. J., R. S. Fraser, and R. A. Ferrare, 1990: Satellite remote sensing of large scale air pollution—method. *J. Geophys. Res.*, **95**, 9895–9909.
- Kaufman, Y. J., R. S. Fraser, and R. L. Mahoney, 1991: Fossil fuel and biomass burning effect on climate—heating or cooling? *J. Climate*, **4**, 578–588.
- Kaufman, Y. J., A. Gitelson, A. Karnieli, E. Ganor, R. S. Fraser, T. Nakajima, S. Mattoo, and B. N. Holben, 1994: Size distribution and phase function of aerosol particles retrieved from sky brightness measurements. *J. Geophys. Res.*, **99**, 10,341–10,356.
- Kiehl, J. T., and B. P. Briegleb, 1993: The relative roles of sulfate aerosols and greenhouse gases in climate forcing. *Science*, **260**, 311–314.
- Kienle, J., K. G. Dean, H. Garbeil, and W. I. Rose, 1990: Satellite surveillance of volcanic ash plumes, application to aircraft safety. *Eos, Trans. Amer. Geophys. Union*, **71**, 266.
- King, M. D., Harshvardhan, and A. Arking, 1984: A model of the radiative properties of the El Chichón stratospheric aerosol layer. *J. Climate Appl. Meteor.*, **23**, 1121–1137.
- King, M. D., L. F. Radke, and P. V. Hobbs, 1993: Optical properties of marine stratocumulus clouds modified by ships. *J. Geophys. Res.*, **98**, 2729–2739.
- King, M. D., Y. J. Kaufman, P. Menzel, and D. Tanré, 1992: Determination of cloud, aerosol, and water vapor properties from the Moderate Resolution Imaging Spectrometer (MODIS). *IEEE Trans. Geosci. Remote Sens.*, **30**, 2–27.
- King, M. D., S. C. Tsay, and S. Platnick, 1995: In situ observations of the indirect effects of aerosol on clouds. *Aerosol Forcing of Climate*, R. J. Charlson and J. Heintzenberg, Eds., John Wiley and Sons, 227–248.
- Kodera, K., and K. Yamazaki, 1994: A possible influence of recent polar stratospheric coolings on the troposphere in the Northern Hemisphere winter. *Geophys. Res. Lett.*, **21**, 809–812.
- Kotra, J. P., D. L. Finnegan, W. H. Zoller, M. A. Hunt, and J. L. Moyers, 1983: El Chichón: Composition of plume gases and particles. *Science*, **222**, 1018–1021.
- Krotkov, N.A., A.J. Krueger, and P.K. Bhartia, 1997: Ultraviolet optical model of volcanic clouds for remote sensing of ash and sulfur dioxide. *J. Geophys. Res.*, **102**, 21,891–21,904.
- Krueger, A.J., L.S. Walter, P.K. Bhartia, C. C. Schnetzler, N.A. Krotkov, I. Sprod, and G.J.S. Bluth, 1995: Volcanic sulfur dioxide measurements from the Total Ozone Mapping Spectrometer (TOMS) instruments. *J. Geophys. Res.*, **100**, 14,057–14,076.
- Labitzke, K., and M. P. McCormick, 1992: Stratospheric temperature increases due to Pinatubo aerosols. *Geophys. Res. Lett.*, **19**, 207–210.
- Labitzke, K., B. Naujokat, and M. P. McCormick, 1983: Temperature effects on the stratosphere of the April 4, 1992 eruption of El Chichón, Mexico. *Geophys. Res. Lett.*, **10**, 24–26.
- Lacis, A. A., and M. Mishchenko, 1995: Climate forcing, climate sensitivity, and climate response: A radiative forcing modeling perspective on atmospheric aerosols. *Aerosol Forcing of Climate*, R. J. Charlson and J. Heintzenberg, Eds., John Wiley and Sons, 11–42.
- Lacis, A. A., J. E. Hansen, and M. Sato, 1992: Climate forcing by stratospheric aerosols. *Geophys. Res. Lett.*, **19**, 1607–1610.
- Lambert, A., R. G. Grainger, J. J. Remedios, C. D. Rodgers, M. Corney, and F. W. Taylor, 1993: Measurements of the evolution of the Mt. Pinatubo aerosol cloud by ISAMS. *Geophys. Res. Lett.*, **20**, 1287–1290.
- Lambert, A., R. G. Grainger, C. D. Rodgers, F. W. Taylor, J. L. Mergenthaler, J. B. Kumer, and S. T. Massie, 1996: Global evolution of the Mount Pinatubo volcanic aerosols observed by the infrared limb-sounding instruments CLAES and ISAMS on UARS. *J. Geophys. Res.*, in press.
- Langner, J., and H. Rodhe, 1991: A global three-dimensional model of the tropospheric sulfur cycle. *J. Atmos. Chem.*, **13**, 225–263.
- Langner, J., H. Rodhe, P. J. Crutzen, and P. Zimmermann, 1993: Anthropogenic influence on the distribution of tropospheric sulphate aerosol. *Nature*, **359**, 712–715.
- Leaich, W. R., J. W. Strapp, G. A. Isaac, and J. G. Hudson, 1986: Cloud droplet nucleation and cloud scavenging of aerosol sulphate in polluted atmospheres. *Tellus*, **38B**, 328–344.
- Leaich, W. R., G. A. Isaac, J. W. Strapp, C. M. Banic, and H. A. Wiebe, 1992: The relationship between cloud droplet number concentrations and anthropogenic pollution observations and climatic implications. *J. Geophys. Res.*, **97**, 2463–2474.
- Lelieveld, J., and J. Heintzenberg, 1992: Sulfate cooling effect on climate through in-cloud oxidation of anthropogenic SO₂. *Science*, **258**, 117–120.
- Lin, X., and J. A. Coakley, Jr., 1993: Retrieval of properties for semi-transparent clouds from multispectral infrared imagery data. *J. Geophys. Res.*, **98**, 18,501–18,514.
- Long, C. S., and L. L. Stowe, 1994: Using the NOAA/AVHRR to study stratospheric aerosol optical thickness following the Mt. Pinatubo eruption. *Geophys. Res. Lett.*, **21**, 2215–2218.
- MacCracken, M. C., and F. M. Luther, 1984: Preliminary estimate of the radiative and climatic effects of the El Chichón eruption. *Geofisica Internacional*, **23**, 385–401.
- Malin, M. C., and M. F. Sheridan, 1982: Computer-assisted mapping of pyroclastic surges. *Science*, **217**, 637–640.
- Malingreau, J., and P. Kaswanda, 1985: Monitoring volcanic eruptions in Indonesia using weather satellite data: The Colo eruption of July 28, 1983. *J. Volcano. Geo. Res.*, **27**, 179–194.
- Martin, G. M., D. W. Johnson, and A. Spice, 1994: The measurement and parameterization of effective radius of droplets in warm stratocumulus clouds. *J. Atmos. Sci.*, **51**, 1823–1842.
- Martonchik, J. V., and D. J. Diner, 1992: Retrieval of aerosol and land surface optical properties from multi-angle satellite imagery. *IEEE Trans. Geosci. Remote Sens.*, **30**, 223–230.

- Massonnet, D., K. Feigl, M. Rossi, and F. Adragna, 1994: Radar interferometric mapping of deformation in the year after the Landers earthquake. *Nature*, **369**, 227–230.
- McCormick, M. P., 1993: Third International Lidar Researchers Directory, Atmospheric Sciences Division, NASA Langley Research Center, Hampton, Virginia.
- McCormick, M. P., 1995: LITE—An overview. 1995 Spring Meeting of the Amer. Geophys. Union, *EOS supplement*, April 25, 67.
- McCormick, M. P., and P. H. Wang, 1987: Satellite measurements of stratospheric aerosols. *Transport Processes in the Middle Atmosphere*, G. Visconti and R. Garcia, Eds., D. Reidel Publishing, 103–120.
- McCormick, M. P., and R. E. Veiga, 1992: SAGE II measurements of early Pinatubo aerosols. *Geophys. Res. Lett.*, **19**, 155–158.
- McCormick, M. P., D. M. Winker, E. V. Browell, J. A. Coakley, C. S. Gardner, R. M. Hoff, G. S. Kent, S. H. Melfi, R. T. Menzies, C. M. R. Platt, D. A. Randall, and J. A. Reagan, 1993: Scientific investigations planned for the lidar in-space technology experiment (LITE). *Bull. Amer. Meteor. Soc.*, **74**, 205–214.
- McCormick, M. P., L. W. Thomason, and C. R. Trepte, 1995: Atmospheric effects of the Mt. Pinatubo eruption. *Nature*, **373**, 399–404.
- Minnis, P., E. F. Harrison, L. L. Stowe, G. G. Gibson, F. M. Denn, D. R. Doelling, and W. L. Smith, 1993: Radiative climate forcing by the Mt. Pinatubo eruption. *Science*, **259**, 1411–1415.
- Mouginis-Mark, P. J., and H. Garbeil, 1993: Digital topography of volcanoes from radar interferometry: An example of Mt. Vesuvius, Italy. *Bull. Volcano.*, **55**, 566–570.
- Muller, J. F., 1992: Geographical distribution and seasonal variation of surface emissions and deposition velocities of atmospheric trace gases. *J. Geophys. Res.*, **97**, 3787–3804.
- Nakajima, T., M. Tanaka, M. Yamano, M. Shiobara, K. Arao, and Y. Nakanishi, 1989: Aerosol optical characteristics in the yellow sand events observed in May, 1982 at Nagasaki-Part 2 Models. *J. Meteor. Soc. Japan*, **67**, 279–291.
- Norris, J. R., and C. B. Leovy, 1995: Comments on “Trends in global marine cloudiness and anthropogenic sulfur.” *J. Climate*, **8**, 2109–2110.
- Novakov, T., and J. E. Penner, 1993: Large contribution of organic aerosols to CCN concentration. *Nature*, **365**, 823–826.
- Osborn, M. T., R. J. DeCoursey, C. R. Trepte, D. M. Winker, and D. C. Woods, 1995: Evolution of the Pinatubo volcanic cloud over Hampton, Virginia. *Geophys. Res. Lett.*, **22**, 1101–1104.
- Parungo, F., J. F. Boatman, H. Sievering, S. W. Wilkinson, and B. B. Hicks, 1994: Trends in global mean cloudiness and anthropogenic sulfur. *J. Climate*, **7**, 434–440.
- Penner, J. E., R. E. Dickinson, and C. A. O’Neill, 1992: Effects of aerosol from biomass burning on the global radiation budget. *Science*, **256**, 1432–1434.
- Pincus, R., and M. Baker, 1994: Effect of precipitation on the albedo susceptibility of marine boundary layer clouds. *Nature*, **372**, 250–252.
- Platnick, S., and S. Twomey, 1994: Determining the susceptibility of cloud albedo to changes in droplet concentration with the Advanced Very High Resolution Radiometer. *J. Appl. Meteor.*, **33**, 334–347.
- Pollack, J. B., O. B. Toon, C. Sagan, A. Summers, B. Baldwin, and W. Van Camp, 1976: Volcanic explosions and climatic change: A theoretical assessment. *J. Geophys. Res.*, **81**, 1071–1083.
- Post, M. J., 1986: Atmospheric purging of El Chichón debris. *J. Geophys. Res.*, **91**, 5222–5228.
- Post, M. J., C. J. Grund, A. O. Langford, and M. H. Proffitt, 1992: Observations of Pinatubo ejecta over Boulder, Colorado by lidars of three different wavelengths. *Geophys. Res. Lett.*, **19**, 195–198.
- Prabhakara, C., R. S. Fraser, G. Dalu, M.-L. C. Wu, and R. J. Curran, 1988: Thin cirrus clouds: Seasonal distribution over oceans deduced from Nimbus-4 IRIS. *J. Climate Appl. Meteor.*, **27**, 279–299.
- Prata, A. J., 1989: Infrared radiative transfer calculations for volcanic ash clouds. *Geophys. Res. Lett.*, **16**, 1293–1296.
- Prospero, J. M., and R. T. Nees, 1976: Dust concentration in the atmosphere of the equatorial North Atlantic: Possible relationship of Saharan drought. *Science*, **196**, 1196–1198.
- Pueschel, R. F., D. F. Blake, K. G. Snetsinger, A. D. A. Hansen, S. Verma, and K. Kato, 1992: Black carbon (soot) aerosol in the lower stratosphere and upper troposphere. *Geophys. Res. Lett.*, **19**, 1659–1662.
- Radke, L. F., D. A. Hegg, P. V. Hobbs, J. D. Nance, J. H. Lyons, K. K. Laursen, P. J. Reagan, and D. E. Ward, 1991: Particulate and trace gas emission from large biomass fires in North America. *Global Biomass Burning: Atmospheric, Climatic, and Biospheric Implications*, J. S. Levine, Ed., MIT Press, 209–224.
- Radke, L. F., J. A. Coakley, Jr., and M. D. King, 1989: Direct and remote sensing observations of the effects of ships on clouds. *Science*, **246**, 1146–1149.
- Rao, C. R. N., L. L. Stowe, and E. P. McClain, 1989: Remote sensing of aerosols over the ocean using AVHRR data: Theory, practice and application. *Int. J. Remote Sens.*, **10**, 743–749.
- Rao, C. R. N., L. L. Stowe, E. P. McClain, J. Sapper, and M. P. McCormick, 1988: Development and application of aerosol remote sensing with AVHRR data from the NOAA satellites. *Aerosols and Climate*, P. V. Hobbs and M. P. McCormick, Eds., A. Deepak Publishing, 69–80.
- Read, W. G., L. Froidevaux, and J. W. Waters, 1993: Microwave limb sounder measurement of stratospheric SO₂ from the Mt. Pinatubo volcano. *Geophys. Res. Lett.*, **20**, 1299–1302.
- Rivera-Carpio, C. A., C. E. Corrigan, T. Novakov, J. E. Penner, C. F. Rogers, and J. C. Chow, 1995: Derivation of contributions of sulfate and carbonaceous aerosol to CCN from mass distributions. Submitted to *J. Geophys. Res.*
- Robock, A., 1983: The dust cloud of the century. *Nature*, **301**, 373–374.
- Robock, A., and M. Matson, 1983: Circumglobal transport of the El Chichón volcanic dust cloud. *Science*, **221**, 195–197.
- Russell, P. B., J. M. Livingston, R. F. Pueschel, J. A. Reagan, E. V. Browell, G. C. Toon, P. A. Newman, M. R. Schoeberl, L. R. Lait, L. Pfister, Q. Gao, and B. M. Herman, 1993a: Post-Pinatubo optical depth spectra vs. latitude and vortex structure: airborne tracking sunphotometer measurements in AASE II. *Geophys. Res. Lett.*, **20**, 2571–2574.
- Russell, P. B., J. M. Livingston, E. G. Dutton, R. F. Pueschel, J. A. Reagan, T. E. DeFoor, M. A. Box, D. Allen, P. Pilewskie, B. M. Herman, S. A. Kinne, and D. J. Hoffman, 1993b: Pinatubo and pre-Pinatubo optical depth spectra: Mauna Loa measurements, comparisons, inferred particle size distributions, radiative effects, and relationship to lidar data. *J. Geophys. Res.*, **98**, 22,969–22,985.
- Sassen, K., 1992: Evidence for liquid-phase cirrus cloud formation from volcanic aerosols: Climatic implications. *Science*, **257**, 516–519.
- Sassen, K., D. O’C. Starr, G. G. Mace, M. R. Poellot, S. H. Melfi, W. L. Eberhard, J. D. Spinhirne, E. W. Eloranta, D. E. Hagen, and J. Hallet, 1995: The 5–6 December 1991 FIRE IFO II jet stream cirrus case study: The influence of volcanic aerosols. *J. Atmos. Sci.*, **52**, 97–123.
- Schneider, S. H., and C. Mass, 1975: Volcanic dust, sunspots, and temperature trends. *Science*, **190**, 741–746.

- Seftor, C. J., N. C. Hsu, J. R. Herman, P. K. Bhartia, O. Torres, W. I. Rose, D. J. Schneider, and N. Krotkov, 1997: Detection of volcanic ash clouds from Nimbus7/Total Ozone Mapping Spectrometer. *J. Geophys. Res.*, **102**, 16,749–16,759.
- Sigurdsson, H., 1990: Assessment of the atmospheric impact of volcanic eruptions. *Global Catastrophes in Earth History*, V. L. Sharpton and P. D. Ward, Eds., Geo. Soc. Amer. paper 247, 99–110.
- Simkin, T., and L. Siebert, 1994: *Volcanoes of the World*, 2nd ed., Geoscience Press, Tucson, 349 pp.
- Simonich, D. M., and B. R. Clemesha, 1995: Comparison between El Chichón and Pinatubo aerosol clouds. IUGG XXI General Assembly, Boulder, Colorado, July 2–14, 1995, Abstracts Week B, p. B250.
- Song, N. D., O' C. Starr, D. J. Wuebbles, K. Kunkel, A. Williams, V. Bowersox, and S. Larson, 1996: Effects of volcanic aerosols on global cloudiness. Submitted to *Science*.
- Spiro, P. A., D. J. Jacob, and J. A. Logan, 1992: Global inventory of sulfur emissions with $1^\circ \times 1^\circ$ resolution. *J. Geophys. Res.*, **97**, 6023–6036.
- Stowe, L. L., P. V. Hobbs, and P. Russell, 1995: Plans for the implementation of the tropospheric aerosol radiative forcing observational experiment. Paper MB52A-12, p. 308 Abstracts for Week B, XXI Assembly IUGG, Boulder Colorado.
- Stowe, L. L., I. M. Ignatov, and R. R. Singh, 1996: Development, validation, and potential enhancements to the second-generation operational aerosol product at NOAA/NESDIS. *J. Geophys. Res.* (in press).
- Strom, J., 1993: *Numerical and airborne experimental studies of aerosol and cloud properties in the troposphere*. Ph.D. thesis, Dept. of Meteorology, Stockholm University.
- Tanré, D., J. F. Geleyn, and J. Slingo, 1984: First results of the introduction of an advanced aerosol-radiation interaction in the ECMWF low resolution global model. *Aerosols and their Climatic Effects*. H. E. Gerber and A. Deepak, Eds., Deepak Publ., 133–177.
- Tanré, D., M. Herman, and Y. J. Kaufman, 1995: Remote sensing of aerosol properties over oceans using the EOS-MODIS reflected spectral radiance: Theoretical approach information on the aerosol size distribution, contained in the reflected spectral radiance of EOS-MODIS. Submitted to *J. Geophys. Res.*
- Taylor, K. E., and J. E. Penner, 1994: Anthropogenic aerosols and climate change. *Nature*, **369**, 734–736.
- Tegen, I., and I. Fung, 1994: Modeling of mineral dust in the atmosphere: Sources, transport, and optical thickness. *J. Geophys. Res.*, **99**, 22,897–22,914.
- Tegen, I., and I. Fung, 1995: Contribution to the atmospheric mineral aerosol load from land surface modification. *J. Geophys. Res.*, **100**, 18,707–18,726.
- Tegen, I., A. A. Lacis, and I. Fung, 1996: The influence of mineral aerosols from disturbed soils on climate forcing. *Nature*, **380**, 419–422.
- Thomason, L. W., 1992: Observations of a new SAGE II aerosol extinction mode following the eruption of Mt. Pinatubo. *Geophys. Res. Lett.*, **19**, 2179–2182.
- Torres, O., P. K. Bhartia, J. R. Herman, Z. Ahmad, and J. Gleason, 1998: Derivation of aerosol properties from satellite measurements of backscattered ultraviolet radiation: Theoretical basis. *J. Geophys. Res.*, **103**, 17,099–17,110.
- Trepte, C. R., and M. H. Hitchman, 1992: The stratospheric tropical circulation deduced from satellite aerosol data. *Nature*, **355**, 626–628.
- Trepte, C. R., L. W. Thomason, and G. S. Kent, 1994: Banded structures in stratospheric aerosol distributions. *Geophys. Res. Lett.*, **21**, 2397–2400.
- Tucker, C. J., H. E. Oregne, and W. W. Newcomb, 1991: Expansion and contraction of the Sahara desert from 1980 to 1990. *Science*, **253**, 299–301.
- Twomey, S. A., 1977: The influence of pollution on the shortwave albedo of clouds. *J. Atmos. Sci.*, **34**, 1149–1152.
- Twomey, S. A., M. Piepgrass, and T. L. Wolfe, 1984: Assessment of the impacts of pollution on the global albedo. *Tellus*, **36B**, 356–366.
- Valero, F. P. J., and P. Pilewskie, 1992: Latitudinal survey of spectral optical depths of the Pinatubo volcanic cloud-derived particle sizes, columnar mass loadings, and effects on planetary albedo. *Geophys. Res. Lett.*, **19**, 163–166.
- Vanderbilt, V. C., L. Grant, L. L. Biehl, and B. F. Robinson, 1985: Specular, diffuse, and polarized light scattered by two wheat canopies. *Appl. Optics*, **24**, 2408–2418.
- Wadge, G., P. A. V. Young, and I. J. McKendrick, 1994: Mapping lava flow hazards using computer simulation. *J. Geophys. Res.*, **99**, 489–504.
- Wang, M., and H. R. Gordon, 1995: Estimation of aerosol columnar size distribution and optical thickness from the angular distribution of radiance exiting the atmosphere: Simulation. *Appl. Opt.*, **33**, 7088–7098.
- Ward, D. E., and C. C. Hardy, 1991: Smoke emissions from wildland fires. *Environment. Intl.*, **17**, 117–134.
- Ward, D. E., R. Susott, J. Kauffman, R. Babbitt, B. N. Holben, Y. J. Kaufman, A. Setzer, R. Rasmussen, D. Cumming, and B. Dias, 1992: Emissions and burning characteristics of biomass fires for cerrado and tropical forest regions of Brazil-BASE-B experiment. *J. Geophys. Res.*, **97**, 14,601–14,619.
- Warner, J., and S. Twomey, 1967: The production of cloud nuclei by cane fires and the effect on cloud droplet concentration. *J. Atmos. Sci.*, **24**, 704–706.
- Winker, D. M., and M. T. Osborn, 1992: Airborne lidar observations of the Pinatubo volcanic plume. *Geophys. Res. Lett.*, **19**, 167–170.
- Yue, G. K., M. P. McCormick, and E. W. Chiou, 1991: Stratospheric aerosol optical depth observed by the Stratospheric Aerosol and Gas Experiment II: Decay of the El Chichón and Ruiz volcanic perturbations. *J. Geophys. Res.*, **96**, 5209–5219.
- Zebker, H. A., P. A. Rosen, R. M. Goldstein, A. Gabriel, and C. L. Werner, 1994: On the derivation of coseismic displacement fields using differential radar interferometry: the Landers earthquake. *J. Geophys. Res.*, **99**, 19,617–19,634.
- Zhao, J., R. P. Turco, and O. B. Toon, 1995: A model simulation of Pinatubo volcanic aerosols in the stratosphere. *J. Geophys. Res.*, **100**, 7315–7328.

Chapter 8 Index

- AATSR 365-366
 ADEOS 366
 AERONET 370
 aerosol abundance 353-354
 aerosol indirect effects of 355-358, 362-366
 aerosol measurements 368-371
 aerosol radiative effects 352-355
 aerosol radiative properties 345-347
 aerosol sources 349-354
 aerosol, climate effects of 349-358, 370-372
 aerosol, climate modification by 372
 agriculture 352, 358
 Agung 342
 aircraft exhaust 350
 aircraft hazards 361-362
 AIRS/AMSU/HSB 367
 ALOS 364-366
 ASTER 361, 364-368
 ATSR 362
 AVHRR 360, 362, 368-369
 biomass burning 341, 350-358, 370-371
 calibration 353, 366, 369-370
 carbon dioxide (CO₂) 348, 359, 369-370
 carbon monoxide (CO) 332, 359, 367
 CCD 369
 CCN 351, 354
 CERES 367
 CHEM-1 368
 chlorine 349
 CLAES 346, 347
 convection 344
 COS 343, 364, 367
 COSEPUP 372
 DEM 359, 361, 365, 365
 DMS 350
 El Chichón 342-344
 El Niño 342, 344, 367
 ENSO 344
 ENVISAT 359, 364-367
 EOS AM 356, 369-371
 EOSP 353, 356, 363-364, 366-371
 EP 368
 ERBE 343, 346
 ERS 360, 366
 ETM+ 367-368
 FAA 360-361
 field campaigns 358
 Franklin, Benjamin 349
 gas-to-particle conversion 343-345
 GISS 346
 GLAS 349, 356, 358, 362-371
 GLI 366
 GOMOS 366
 GPS 362
 H₂SO₄ 342-343, 345-346
 HCl 342, 358-359, 364, 367
 health hazards, volcanic 359-361
 HIRDLS 347, 362-363, 366-367
 HSB 367
 humidity 350, 367
 ICESat 356, 371
 IDS 362, 367
 ILAS 366
 IPCC 350-352, 370
 IR 365, 368
 ISAMS 346-347
 JERS 366
 Krakatau 342, 344
 lidar 344, 347-349, 356, 367, 371
 MERIS 366
 METEOR-3 347, 368
 MISR 353-357, 362-371
 MLS 345, 363-364, 367
 modeling 345, 371
 MODIS 353, 356, 362-370
 Mt. Katmai 342
 Mt. Pinatubo 343-348, 361, 366-367, 371
 Mt. Saint Helens 344
 MSU 343-344
 NASA 366
 Nevada del Ruiz 344
 NOAA 368
 NO_x 350
 ocean circulation 341, 366
 OCTS 366
 OLR 344
 OMI 350, 355-356, 363-365
 POLDER 366
 precipitation 343-344
 QBO 344
 RADARSAT 359, 364, 366
 SAGE 350
 SAGE II 347
 SAGE III 347, 363, 367
 salinity 359
 SAM 349
 SAR 362, 364
 SCANSAR 366
 SCF 363
 sulfate 41-352, 359, 365, 370-371
 sulfur 341-343, 351
 sulfur dioxide (SO₂) 41-346, 350-354, 358-359, 365, 367-368
 sulfuric acid 342-343, 345-346
 SW 347
 SWIR 365, 369-370
 Tambora 342, 344
 TARFOX 353
 TIR 362, 365
 TOMS 356, 365, 367-369
 topography 361-367
 TOPSAR 361
 trace gases 350-351
 validation 349, 366, 370
 VOC 350-351
 volcanic detection 360-362, 368
 volcanic hazards 358-362, 367
 volcanic measurements, international 368
 volcanoes 341-372
 water vapor 342-345, 350, 352, 358, 362, 364, 368
 wind 341, 344, 367, 370
 year without a summer 342